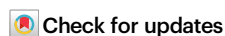


Crinophagic granules in pancreatic β cells contribute to mouse autoimmune diabetes by diversifying pathogenic epitope repertoire

Received: 11 December 2023

Accepted: 13 September 2024

Published online: 27 September 2024




Hao Hu ^{1,7}, Anthony N. Vomund^{1,2,7}, Orion J. Peterson^{1,2}, Neetu Srivastava^{1,2}, Tiandao Li ³, Lisa Kain ⁴, Wandy L. Beatty⁵, Bo Zhang ³, Chyi-Song Hsieh⁶, Luc Teyton ⁴, Cheryl F. Lichti ^{1,2}, Emil R. Unanue ^{1,2,8} & Xiaoxiao Wan ^{1,2} 

Autoimmune attack toward pancreatic β cells causes permanent loss of glucose homeostasis in type 1 diabetes (T1D). Insulin secretory granules store and secrete insulin but are also thought to be tissue messengers for T1D. Here, we show that the crinophagic granules (crinosome), a minor set of vesicles formed by fusing lysosomes with the conventional insulin dense-core granules (DCG), are pathogenic in T1D development in mouse models. Pharmacological inhibition of crinosome formation in β cells delays T1D progression without affecting the dominant DCGs. Mechanistically, crinophagy inhibition diminishes the epitope repertoire in pancreatic islets, including cryptic, modified and disease-relevant epitopes derived from insulin. These unconventional insulin epitopes are largely undetectable in the MHC-II epitope repertoire of the thymus, where only canonical insulin epitopes are presented. CD4⁺ T cells targeting unconventional insulin epitopes display autoreactive phenotypes, unlike tolerized T cells recognizing epitopes presented in the thymus. Thus, the crinophagic pathway emerges as a tissue-intrinsic mechanism that transforms insulin from a signature thymic self-protein to a critical autoantigen by creating a peripheral-thymic mismatch in the epitope repertoire.

Type 1 diabetes (T1D) is orchestrated by antigen-specific T cells that selectively target and destroy pancreatic β cells within the islets of Langerhans. The occurrence of T1D is predominantly determined by certain major histocompatibility class II (MHC-II) alleles expressed in genetically predisposed individuals^{1,2}. This association indicates that T1D initiation is not a stochastic event but rather programmed by MHC-II presentation of islet-derived antigens to self-reactive CD4⁺

T cells. As the sole cell type responsible for controlling systemic glucose levels, β cells employ sophisticated molecular pathways to accomplish insulin biosynthesis and secretion, processes that mainly take place in secretory granules with the involvement of numerous enzymes, intermediates, and proteins. A range of proteins or polypeptides associated with β -cell secretory granules, such as insulin, chromogranin A (ChgA), islet amyloid polypeptide (IAPP), islet

¹Department of Pathology and Immunology, Division of Immunobiology, Washington University School of Medicine, St. Louis, MO, USA. ²The Andrew M. and Jane M. Bursky Center for Human Immunology and Immunotherapy Programs, Washington University School of Medicine, St. Louis, MO, USA. ³Department of Developmental Biology, Center of Regenerative Medicine, Washington University School of Medicine, St. Louis, MO, USA. ⁴Department of Immunology and Microbiology, Scripps Research Institute, La Jolla, CA, USA. ⁵Department of Molecular Microbiology, Washington University School of Medicine, St. Louis, MO, USA. ⁶Department of Internal Medicine, Division of Rheumatology, Washington University School of Medicine, St. Louis, MO, USA. ⁷These authors contributed equally: Hao Hu, Anthony N. Vomund. ⁸Deceased: Emil R. Unanue.  e-mail: wanx@wustl.edu

antigen-2 (IA-2), and zinc transporter 8 (ZnT8), have emerged as autoantigens in T1D³, supporting the notion that normal β -cell functions can precipitate T1D pathogenesis before the overt manifestation of β -cell dysfunction and failure⁴.

The non-obese diabetic (NOD) mouse strain has provided an experimental platform for investigating antigens involved in the initiation stage of T1D. The NOD mouse is a spontaneous autoimmune model in which diabetes development is dictated by its expression of a single MHC-II molecule, I-A^{g7.5}, a structural analog to the human susceptible haplotype HLA-DQ8^{6–8}. Utilizing the NOD model, fundamental studies have identified insulin as a primary initiating antigen in T1D^{9,10}. MHC-II presentation of insulin has been shown to foster autoantibody, B-cell, and T-cell responses, which appear long before terminal clinical diabetes^{5,11–14}. Genetic manipulation of insulin gene expression is sufficient to alter disease outcomes^{15–22}, suggesting that insulin autoreactivity precedes and is likely a prerequisite for triggering downstream epitope spreading. Despite such compelling evidence, the identification of insulin as a major autoantigen is somewhat unexpected. Insulin is a small (5.8 kDa) molecule that provides only limited epitopes for T-cell recognition. Moreover, insulin is one of the earliest self-proteins known to be expressed by medullary thymic epithelial cells (mTECs)²³. These findings raise a conundrum, pointing to an incomplete understanding of mechanisms that transform insulin, a signature thymic protein, into a crucial autoantigen.

In β cells, insulin is condensed into a crystalline core for storage in the regular secretory granules. At the steady state, a β cell contains about 10,000 of these dense-core granules (DCGs). A small fraction of DCGs was observed to fuse with lysosomes, forming a different set of vesicles termed as crinophagic bodies or crinosomes^{24–26}. This crinophagic pathway is thought to be an energy-efficient process by which endocrine cells dispose of excessive secretory granules²⁷. In contrast to DCGs that store insulin, crinosomes mainly contain degraded insulin peptide segments²⁸. Such a distinction in granule contents corresponds to immunological evidence showing that intact insulin elicits little T-cell responses, whereas free insulin peptides are highly immunogenic^{29,30}. Additionally, crinosomes may also facilitate the formation of disease-relevant neoantigens, such as hybrid insulin peptides (HIPs), owing to their more acidic microenvironment and high enzymatic activity^{31–33}. These results suggest that crinophagy serves as a β -cell intrinsic mechanism underlying the generation and diversification of potentially pathogenic epitopes. Whether this minor set of the crinophagic granules contributes to T1D development, a pathogenic role that unfolds independently from the dominant DCGs, remains to be determined.

In this study, we use a pharmacological approach to target crinophagy without having a detectable impact on DCGs. Crinophagy inhibition reduces the abundance and diversity of the epitope repertoire in β cells, leading to diminished MHC-II presentation of insulin epitopes in vivo and suppression of diabetes development in NOD mice. Mechanistically, we focus on examining whether crinophagy fosters the generation of a local epitope repertoire in pancreatic islets that deviates from the thymic repertoire, using a multivariate approach integrating immunopeptidomics, antigen presentation assay and single-cell analysis of antigen-specific CD4⁺ T cells recognizing MHC-II epitopes presented in the thymus versus islets. These studies not only identify the physiological crinophagic pathway as a novel pathogenic element in T1D but also provide further explanations as to why insulin autoreactivity takes place despite efficient central tolerance.

Results

Crinophagy plays a pathological role in T1D development

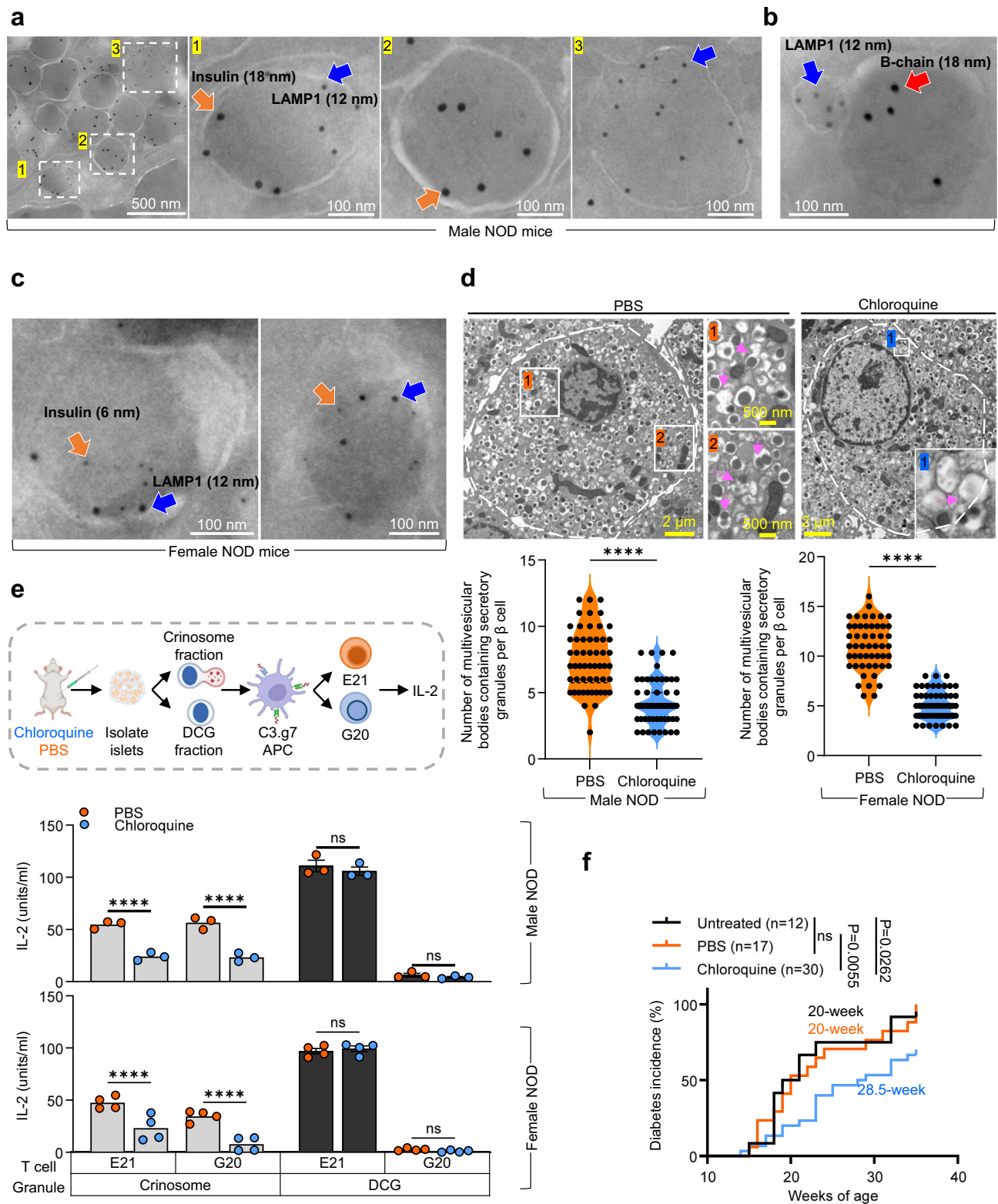
Crinosomes in pancreatic β cells are described as multivesicular bodies containing secretory granules when examined by regular electron microscopy^{24,26}. To visualize crinosomes with specific markers, we

performed immunogold electron microscopy on purified mouse islets using primary anti-insulin or anti-LAMP1 antibodies, followed by labeling with secondary antibodies conjugated with colloidal gold of different sizes. Given that crinophagy is a physiological process, we first assessed young male NOD mice when most islets are inflammation-free. We identified three sets of vesicular structures that were differentially labeled with insulin (18 nm gold) and LAMP1 (12 nm gold) in the same β cell (Fig. 1a). Crinosomes were indicated as granular structures that were co-labeled with both insulin and LAMP1 (Fig. 1a). These structures coexisted with vesicles containing insulin or LAMP1 alone (Fig. 1a), which represented the conventional insulin dense-core granules (DCGs) and lysosomes, respectively. Since crinosomes are characterized by their content of catabolized insulin peptides, we further employed a peptide-specific antibody (clone 6F3) exclusively recognizing peptide segments of the insulin B-chain but not the intact insulin molecule²⁸. This approach also revealed granule structures containing both insulin B-chain peptides and LAMP1, indicating the presence of crinosomes (Fig. 1b). We then verified these results using islets from 4-week-old female NOD mice when small numbers of initial T cells can be found in the islets³⁴. We used a smaller gold particle to visualize insulin and observed crinosome-like vesicles containing both insulin (6 nm gold) and LAMP1 (12 nm gold) (Fig. 1c). Collectively, these data confirmed that crinosomes are a specific set of lysosome-associated granules containing degraded insulin products, which can be detected at the initial phase of autoimmune diabetes development in NOD mice.

Next, we explored the possibility of inhibiting the generation of crinosomes in young male and female NOD mice. In β cells, crinophagy is considered a form of autophagy specialized for catabolizing secretory granules. Given that chloroquine has been previously shown to inhibit the formation of autophagolysosomes by impairing the fusion of autophagosomes to lysosomes without affecting the acidification of these organelles^{35,36}, we hypothesized that it may similarly impair the fusion of DCG to lysosomes when acting on β cells, thereby decreasing crinosome generation. Considering that crinosomes may have a rapid turnover rate, we used a short-term protocol in which four doses of chloroquine were administered by intraperitoneal injections over a three-day period to 6-week-old male or 4-week-old female NOD mice. Pancreatic islets were then isolated and examined by regular electron microscopy. In mice given either chloroquine or PBS control, we observed a prominent presence of the typical DCGs in β cells (Fig. 1d). Although the irregular multivesicular secretory granules representing crinosomes constituted only a minor portion of total granules in β cells, these crinosome-like vesicles were reduced by half in both male and female NOD mice given the chloroquine treatment (Fig. 1d).

Considering that in vivo administration of chloroquine may have broad effects in other cells, we used an antigen presentation assay to directly assess the impact of the chloroquine treatment on crinosomes and DCGs. We isolated subcellular fractions representing crinosomes or DCGs from equal numbers of β cells from young male and female NOD mice given the short-term treatment with chloroquine or PBS, using a protocol based on differential centrifugation^{28,37}. The freshly isolated granule fractions were exposed to the I-A^{g7}-expressing B-cell lymphoma C3.g7, followed by addition of two I-A^{g7}-restricted CD4⁺ T cell hybridomas (9B9 and IIT-3), to probe the presentation of granule-derived insulin epitopes by the C3.g7 APC (Fig. 1e).

This system leverages distinct reactivities between the 9B9 and IIT-3 T cells, allowing for quantitative assessment of the level of intact insulin versus free peptides in the granule fractions. The 9B9 T cell specifically recognizes the insulin B-chain 12–20 epitope (G20, VEA-LYLVCG), which can only be presented when APCs are offered free insulin peptides but not intact insulin^{29,30}. In contrast, the IIT-3 T cell is specific for the 13–21 epitope (E21, EALYLVCGE), which is presented when APCs handle either insulin peptides or intact insulin^{29,30}. When



stimulated with synthetic peptides containing either the G20 (Syn-G20; TEGVEALYLVCGGGS) or the E21 (Syn-E21; TEGEALYLVCGECS) binding core with identical flanking residues, the two hybridomas exclusively reacted to their corresponding epitopes (Supplementary Fig. 1a). Only the IIT-3 but not the 9B9 T cell responded to C3.g7 pulsed with intact insulin (Supplementary Fig. 1a). Both T cells showed similar responses to the native insulin B:9-23 peptide (SHLVEALYLVCGERG) containing both registers (Supplementary Fig. 1b), demonstrating their comparable sensitivities.

Using this antigen presentation assay, we previously found that the subcellular fraction obtained via 5000g was the only fraction capable of presenting the G20 epitope, suggesting that this “5k” fraction is particularly enriched for insulin peptide fragments and represents crinosomes. In contrast, the fraction obtained via 25,000g (25k), only presented the E21 epitope, indicating that it mainly represented DCGs containing insulin molecules³⁷. These results were later verified by examining granule contents through ELISA and mass spectrometry analysis²⁸.

Fig. 1 | Disruption of the crinophagic pathway in pancreatic β cells leads to suppression of autoimmune diabetes development in NOD mice.

a Immunogold electron microscopy depicting vesicles differentially labeled for insulin (18 nm, indicated by red arrow) and LAMP1 (12 nm, indicated by blue arrow) in a β -cell from 6-week-old male NOD mice. Also shown are three individual granules, some containing both insulin and LAMP1, while others contain only insulin or LAMP1. Data are representative of two independent experiments. **b** Immunogold electron microscopy depicting a representative granule containing both insulin B-chain (18 nm, indicated by red arrow) and LAMP1 (12 nm, indicated by blue arrow) from 6-week-old male NOD mice. Data are representative of two independent experiments. **c** Immunogold electron microscopy depicting two representative granules containing both insulin (6 nm, indicated by red arrow) and LAMP1 (12 nm, indicated by blue arrow) from 4-week-old female NOD mice. Data are representative of two independent experiments. **d** Representative electron microscopy images showing β cells from 6-week-old male NOD mice post-treatment with chloroquine or PBS control (upper). The data show randomly selected regions from a β cell. In each region, crinophagic granules, which have the morphology of multivesicular bodies containing secretory granules, are denoted by purple arrows.

For further validation, we analyzed 5k, 15k (obtained via 15,000g), and 25k subcellular fractions (from islets of 4-week-old female NOD mice) for both antigen presentation and acid phosphatase levels (to measure lysosome activity) (Supplementary Fig. 1c). Presentation of G20 was again seen only in the 5k but not the 25k fraction, whereas the 25k fraction only presented E21 (Supplementary Fig. 1d). Also, the 5k but not the 25k fraction exhibited acid phosphatase activity (Supplementary Fig. 1e). Although presentation of either G20 or E21 was minimal in the 15k fraction (Supplementary Fig. 1d), we detected acid phosphatase in the 15k fraction (Supplementary Fig. 1e), suggesting the presence of lysosomes in this fraction. We also observed similar total protein levels in these granule fractions isolated from age/sex-matched NOD and diabetes-resistant B6g7 (B6 mice expressing I-Ag7) mice (Supplementary Fig. 1f). Presentation of G20 and E21 in the crinosome and DCG fractions was also comparable between the two strains (Supplementary Fig. 1g). Overall, these results confirm that the 5k fraction, as the only fraction having both insulin peptide production and lysosome activity, is compatible with features of crinosomes. Furthermore, the minimal antigen presentation in the 15k fraction suggested that the isolation of the crinosome fraction had minimal mixing with lysosomes.

We observed consistent effects of chloroquine between male and female NOD mice (Fig. 1e). In mice given PBS, presentation of the G20 epitope was only observed in the crinosome but not the DCG fraction, confirming that crinosomes are particularly enriched for free insulin peptides (Fig. 1e). Notably, treatment with chloroquine resulted in a ~50% reduction in the presentation level of both G20 and E21 in the crinosome fraction (Fig. 1e), a finding in line with the electron microscopy results showing the reduction of crinosomes. In contrast to crinosomes, the DCG fraction predominantly presented the E21 epitope, while the level of G20 was minimal (Fig. 1e), indicating its primary content of insulin molecules. Furthermore, the chloroquine treatment did not influence the presentation of both epitopes in DCGs (Fig. 1e). These results demonstrated that chloroquine caused a reduction in the production of catabolized insulin peptides in β cells. More importantly, the effect was specific to crinosomes, with minimal impact on DCGs.

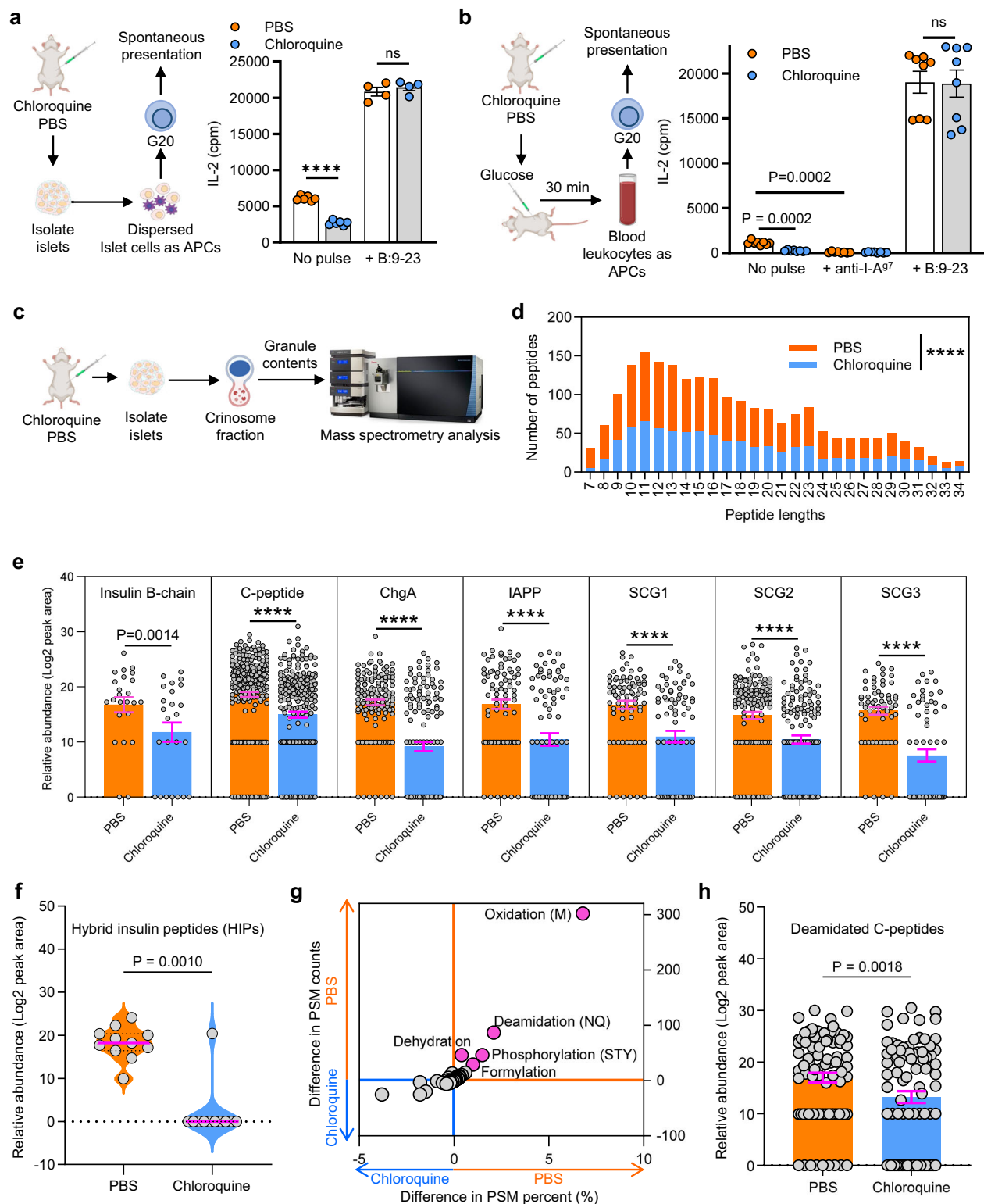
Free insulin peptides that give rise to the G20 epitope were shown to be highly immunogenic in NOD mice, whereas T-cell responses to intact insulin (E21) were largely undetectable^{29,30}. Whether this pathogenic outcome relates to the physiological role of crinosomes remains undetermined. We reasoned that chloroquine treatment might represent a feasible experimental approach to address this question, based on the results that it decreased the formation of crinosomes. Moreover, although chloroquine is known to inhibit internal processing of protein antigens by APCs, it did not influence the capacity of

The violin plots (lower) summarize the numbers of the crinophagic granules per β cell in 6-week-old male or 4-week-old female NOD mice. Data are from two independent experiments. Each symbol represents individual β cells. **** $P < 0.0001$; Mann–Whitney test, two-tailed. **e** Schematic (upper) depicting an antigen presentation assay designed for testing the presentation of the insulin epitope G20 or E21 contained in crinosome or DCG subcellular fractions isolated from islets of NOD mice given PBS or chloroquine. Created in BioRender. Wan, X. (2024) BioRender.com/w12p880. The bar graphs (lower) summarize results (mean \pm s.e.m) from three or four independent experiments in 6-week-old male or 4-week-old female NOD mice. Each symbol represents one independent experiment including 2–5 mice pooled together (for experiment for males: $n = 15$ in total; for experiment for females: $n = 16$ in total). ns, not significant; **** $P < 0.0001$; one-way ANOVA analysis. **f** Diabetes development of female NOD mice that were left untreated ($n = 12$) or treated with PBS ($n = 17$) or chloroquine ($n = 30$). The median age of diabetes onset for each group is indicated. Diabetes incidence was determined by three independent monitoring experiments. ns not significant; ** $P = 0.0055$; * $P = 0.0262$; Log-rank (Mantel–Cox) test.

APCs to present already-processed extracellular insulin peptides^{31,37}, materials that bypass internal processing. Given that excessive inhibition of the crinophagic pathway may cause adverse effects, we developed an intermittent treatment regimen in which chloroquine was administered twice a week for three weeks, followed by a 1-week break. We started the intermittent treatment cycle in 3-week-old female NOD mice to target crinophagy before potential β -cell dysfunction and monitored diabetes incidence up to 35 weeks of age. Both untreated mice and mice given PBS showed a median onset of hyperglycemia by 20 weeks of age, whereas treatment with chloroquine delayed diabetes onset (median 28.5 weeks of age) (Fig. 1f). Diabetes incidence in the untreated mice was similar to other female mice in our monitoring cages (Supplementary Fig. 1f), which exhibited progressive insulinitis development (Supplementary Fig. 1g), suggesting minimal genetic drift in our colony. Additionally, while all the PBS-treated mice eventually became diabetic, about 33% of mice in the chloroquine group remained diabetes free by 35 weeks of age (Fig. 1f). These results suggest that targeting crinophagy from the initial disease stage can impede T1D progression with diminished epitope production serving as a contributing mechanism.

Inhibiting crinophagy reduces the epitope repertoire in pancreatic islets

Having demonstrated that chloroquine treatment resulted in a reduction of crinosomes in β cells and a delay in diabetes development, we next sought to determine whether inhibiting crinophagy could directly impact the MHC-II presentation of insulin epitopes in vivo. Our previous studies identified two major sites for the presentation of crinosome-derived insulin peptides to CD4⁺ T cells: pancreatic islets and various secondary lymphoid organs (SLOs)^{13,28,31,37,38}. To investigate the local presentation in islets, we examined the role of the islet resident macrophages, the primary APC that reside in the pancreatic islets from birth³⁹. Islet macrophages are characterized by their high expression of MHC-II molecules and their close interactions with β cells^{40,41}. These features allow the islet macrophages to actively sample and present antigenic products from β cells. Depletion of islet macrophages largely abolished diabetes development in NOD mice, underscoring their crucial role in the pathogenic process⁴². To assess in vivo presentation by islet macrophages, we utilized dispersed islet cells from 6-week-old male or 4-week-old female NOD mice, in which islet macrophages were shown to constitute about 95% of the CD45⁺ immune cell population^{34,38,40,43}. Specifically, islets isolated from mice given chloroquine or PBS were non-enzymatically dispersed, and the dispersed islet cells were cultured with the 9B9 T cell in the absence of exogenous antigens to probe changes in the spontaneous presentation of the G20 epitope (Fig. 2a). We observed a substantial decrease



(~50%) in the spontaneous presentation of G20 in the islets from either male (Fig. 2a) or female (Supplementary Fig. 2a) mice given chloroquine compared to those given PBS. Importantly, no difference in G20 presentation was observed when dispersed islet cells were pulsed with exogenous B:9-23 peptide (Fig. 2a; Supplementary Fig. 2a), confirming that chloroquine did not alter the intrinsic capacity of APCs to present extracellular insulin peptides. Thus, inhibiting crinophagy in β

cells led to a decrease in the local MHC-II presentation of the immunogenic G20 epitope by the islet resident macrophages.

Peripheral T-cell priming is essential for T1D development in NOD mice^{44,45}. As a step for sensitizing peripheral lymphoid tissues, insulin peptides derived from crinosomes are released into the circulation following β -cell degranulation triggered by in vivo glucose stimulation^{28,46}. These peptides are rapidly captured by MHC-II⁺ blood

Fig. 2 | Crinophagy inhibition diminishes in vivo insulin presentation and reduces the epitope repertoire in pancreatic islets. **a** Presentation of G20 by dispersed islet cells (islet resident macrophages) from 6-week-old male NOD mice given PBS or chloroquine without antigen pulse or during pulse with the B:9–23 peptide (10 μ M). Data (mean \pm s.e.m) summarize results from three independent experiments; each symbol represents one biological replicate, with 2–5 mice pooled together (for the no antigen pulse group, $n = 30$; for the peptide pulse group, $n = 8$). ns, not significant; $^{**}P = 0.0022$; Mann–Whitney test, two-tailed. A schematic figure is created in BioRender. Wan, X. (2024) BioRender.com/s20b261. **b** Spontaneous presentation of G20 by blood leukocytes isolated from 6-week-old male NOD mice given PBS or chloroquine without antigen pulse or during pulse with the B:9–23 peptide (10 μ M). The specificity of MHC-II presentation was tested by adding the anti-I-A^{B7} blocking antibody to the culture. Data (mean \pm s.e.m) summarize results from four independent experiments; each symbol represents results from an individual mouse ($n = 8$). ns not significant; $^{***}P = 0.0002$; Mann–Whitney test, two-tailed. A schematic figure is created in BioRender. Wan, X. (2024) BioRender.com/s20b261. **c** Schematic for assessing the crinosome

peptidome, created in BioRender. Wan, X. (2024) BioRender.com/s20b261. Each condition (PBS or chloroquine) included 1.2×10^6 live beta cells from ~1500 islets purified from 10 mice. **d** The number of individual peptide sequences at indicated lengths identified in the peptidome of the crinosomes subcellular fraction from islets of NOD mice given PBS or chloroquine. $^{****}P < 0.0001$; two-way ANOVA analysis. **e** Relative abundance of individual peptides (each symbol) belonging to indicated β -cell secretory proteins in the crinosome peptidomes (mean \pm s.e.m). The comparisons were made between PBS and Chloroquine groups within each individual protein. $^{**}P = 0.0014$; $^{****}P < 0.0001$; Wilcoxon test, two-tailed. The numbers of peptides from each protein are Insulin B-chain: 24; C-peptide: 261; ChgA: 133; IAPP: 79; SCG1: 73; SCG2: 131; SCG3: 60. **f** Relative abundance of individual HIPs (each symbol) in the crinosome peptidomes. $^{***}P = 0.0010$; Wilcoxon test, two-tailed. **g** PTM analysis in the crinosome peptidomes. Denoted are several PTMs with a higher presence in the crinosome peptidome from PBS-treated mice versus those given the chloroquine treatment. **h** Relative abundance of individual deamidated C-peptides (each symbol) in the crinosome peptidomes (mean \pm s.e.m). $^{**}P = 0.0018$; Wilcoxon test, two-tailed. Number of peptides detected: 11.

leukocytes, primarily circulating B cells, within a brief time frame (2 h) post glucose challenge, resulting in weak but detectable levels of spontaneous MHC-II presentation⁴⁶. Following short-term treatment with chloroquine or PBS, 6-week-old male or 4-week-old female NOD mice were given a glucose challenge, and the blood leukocytes were isolated 30 min later for antigen presentation assay (Fig. 2b). In both male (Fig. 2b) and female (Supplementary Fig. 2b) NOD mice, we detected spontaneous presentation of G20 by blood leukocytes from PBS-treated mice. Such presentation was blocked by anti-I-A^{B7} antibody, confirming its dependence on MHC-II (Fig. 2b). Notably, chloroquine treatment significantly inhibited the spontaneous presentation of G20 by the blood leukocytes without affecting the presentation during pulse with exogenous B:9–23 (Fig. 2b; Supplementary Fig. 2b). Thus, the chloroquine treatment also diminished circulatory insulin peptides derived from crinosomes, which may lead to reduced presentation in peripheral lymphoid tissues.

The observation of reduced insulin peptide presentation in both islets and circulation prompted us to explore how the chloroquine treatment might broadly alter the epitope repertoire in crinosomes. To assess the crinosome peptidome, we isolated crinosome fractions from equal numbers of β cells from NOD mice given the short-term treatment with chloroquine or PBS control; the granule contents were released through repeated cycles of freezing and thawing and then analyzed by mass spectrometry (MS; Fig. 2c). Peptides from both chloroquine- and PBS-treated mice showed a similar pattern of length distribution, with the majority falling into the 10–18 residue range (Fig. 2d). However, a significant reduction was observed in the number of peptides spanning the entire length distribution of the peptidome within crinosomes isolated from chloroquine-treated mice (Fig. 2d).

We analyzed native peptide sequences originating from β -cell secretory proteins, including insulin (both B-chain and C-peptide), ChgA, IAPP, and secretogranin-1 (SCG1), -2 (SCG2), and -3 (SCG3). The relative abundance (measured by MS peak area under the curve) of individual peptides belonging to each of these proteins showed a consistent and significant decrease in the crinosome peptidome from chloroquine-treated mice (Fig. 2e). These results demonstrated that in vivo chloroquine administration led to a global decline in the production of peptides derived from β -cell secretory proteins in the crinosomes.

In addition to native peptides, we assessed the production of hybrid insulin peptides (HIPs) in the crinosome peptidome. HIPs have been shown to be strong agonists to pathogenic CD4⁺ T cell clones^{47–49}. As an acidic vesicle compartment rich in peptide segments, crinosomes have been implicated as a site for HIP formation in β cells. To assess the impact of the chloroquine treatment on HIP generation, we performed a multi-round search in the crinosome peptidomes using an in silico HIP database⁵⁰, followed by stringent validation as previously

suggested^{31,51}. We initially identified 11 putative HIPs in crinosomes from PBS-treated mice. To verify these assignments, we appended these HIP sequences to the Uniprot-Mouse database and repeated the search as before. Ten out of the eleven HIPs were identified again (Supplementary Fig. 2c). The identified HIP sequences comprised insulin C-peptides joined by different segments from C-peptide or IAPP and could be categorized into five families based on sequence similarities (Supplementary Fig. 2c). Moreover, we validated the longest form of sequences in each family, all of which showed a complete match to their synthetic standards (Supplementary Fig. 2d). Notably, using the same criteria, only one HIP (with an identical sequence to one HIP from the PBS control sample) was identified in crinosomes from mice given chloroquine (Supplementary Fig. 2c). The overall HIP abundance showed a significant decrease in crinosomes from chloroquine-treated mice (Fig. 2f).

The observation of diminished HIP generation led us to further analyze peptides with post-translational modifications (PTMs). Through a PEAKS PTM search that considers 312 entries in the Unimod database, we identified 129 PTMs in the crinosome peptidomes from mice given PBS or chloroquine. We compared peptide-spectra matches (PSMs) belonging to each PTM (both raw counts and percentage) between the two conditions and found several PTMs that were reduced in mice given chloroquine, such as methionine oxidation, deamidation, dehydration, phosphorylation, and formylation (Fig. 2g).

While dehydration, formylation, and methionine oxidation can be artifacts of sample preparation³¹, previous studies have noted a role of phosphorylation in forming neoepitopes during cancer immunity^{52,53} and the contribution of deamidation in the pathogenesis of T1D in NOD mice³¹. Native insulin C-peptide has been identified as a T1D-relevant autoantigen in both NOD mice and humans^{31,54}. In the crinosome peptidomes, we identified C-peptides containing phosphorylation (phosphorylated serine) and deamidation (Q-to-E conversion). Most of these harbored either phosphorylation or deamidation, with few containing both (see an example in Supplementary Fig. 3a). To test whether phosphorylation may modify T cell responses to the native C-peptide, we immunized NOD mice with the native full-length insulin-1 (encoded by the *Ins1* gene) C-peptide and assessed T cell responses upon recall with the native, phosphorylated, or deamidated C-peptide by ELISPOT (Supplementary Fig. 3b). We did not observe notable changes in the production of IL-2 and IFN γ by the phosphorylated C-peptide relative to its native counterpart (Supplementary Fig. 3b). In contrast, deamidated C-peptide significantly enhanced T-cell responses (Supplementary Fig. 3b). A similar profile was also observed when NOD mice were immunized with a mixture of the phosphorylated and deamidated C-peptides (Supplementary Fig. 3b). Thus, unlike deamidation that amplifies autoreactivity to mouse C-peptide, the identified phosphorylation showed minimal effects in altering T cell responses.

We previously identified various sequences of deamidated C-peptides in the MHC-II peptidome of pancreatic islets³¹. Based on these findings, we assessed the relative abundance of all the deamidated insulin C-peptides and found a significant reduction in the crinosome peptidome of chloroquine-treated mice (Fig. 2h). Thus, in addition to the overall reduction in peptide abundance, the chloroquine treatment further diminished the generation of disease-relevant PTMs in crinosomes, supporting its role in restricting the pathogenic epitope repertoire in pancreatic islets.

Thymus lacks presentation of insulin epitopes derived from crinosomes

Our results indicated that crinosomes, despite being a minor set of granules in β cells, contribute to the pathogenesis of autoimmune diabetes. These findings echoed early studies proposing that self-tolerance to the insulin molecule is well-established, whereas already-processed insulin products confer autoreactivity, a phenomenon relating to two distinct modes of antigen presentation^{29,30}. Specifically, MHC-II presentation of intact insulin follows the canonical intracellular pathway in which the stronger-binding E21 epitope is selectively presented, whereas weak-binding epitopes like G20 are eliminated through epitope editing (by H2-DM) in late endosomal compartments. Conversely, APCs handle extracellular insulin peptides in early or recycling endosomes where epitope editing mechanisms are absent. This less constrained, non-canonical presentation mode allows the presentation of the otherwise excluded epitopes, such as G20. In addition to G20 in T1D, autoimmune T-cells specific for transthyretin in juvenile idiopathic arthritis⁵⁵ or hypocretin in narcolepsy⁵⁶ only responded to antigens in the form of free peptides rather than intact proteins. CD4⁺ T cells to these cryptic epitopes are thought to escape thymic selection; however, this hypothesis has not been tested in vivo using bona fide MHC-II epitopes presented in the thymus.

To address this question, we sought to determine which insulin epitopes are naturally present in the thymus. Insulin is estimated to be expressed by only 1–3% of medullary thymic epithelial cells (mTECs) at a given time⁵⁷. To directly assess the presentation of low-abundance insulin epitopes, we FACS-sorted I-A^{B7}-expressing mTECs from 3 to 6-week-old NOD mice (Supplementary Fig. 4a) and cultured them with different insulin-specific CD4⁺ T cell hybridomas in the absence of exogenous antigens (Fig. 3a). Our analysis included the two insulin B-chain epitopes (G20 and E21) as well as two epitopes from the C-peptide (CP1 and CP2), all known to bind I-A^{B7} (ref. 31; Fig. S4b).

Using the 9B9 and IIT-3 T cells, we observed that mTECs isolated from WT NOD mice exhibited spontaneous presentation of the E21 epitope, while the presentation of G20 was at the background level (Fig. 3b). To confirm the specificity of this low-level presentation, we tested I-A^{B7}-expressing mTECs isolated from the NOD.B16A mice, which harbor a Y16A substitution in the B:9–23 peptide that abolishes anti-insulin T cell reactivity diabetes development²². Indeed, minimal spontaneous presentation of E21 or G20 was observed in mTECs from the NOD.B16A mice (Fig. 3b), demonstrating the specificity of the presentation of the E21 epitope observed in mTECs from WT NOD mice.

The selective presentation of the E21 epitope suggested that mTECs mainly have access to insulin protein but not processed peptide fragments. Supporting this notion, we previously found that fluorescently labeled B:9–23 peptide was mostly captured by peripheral APCs, such as splenic B cells and DCs, rather than by thymic APCs, following intravenous injection²⁸. This finding indicated limited access to blood-derived insulin peptides to thymic APCs²⁸. To confirm this, we pulsed mTECs isolated from NOD or NOD.B16A mice with intact insulin and observed a strong presentation of E21, whereas presentation of G20 was minimal (Fig. 3c). In contrast when the mTECs were exposed to B:9–23 as a free peptide, both registers were presented at a high level (Fig. 3c). These results suggest that mTECs utilize a presentation

mode similar to that previously seen in professional APCs and that mTECs spontaneously present E21 through their internal processing of insulin.

In addition to B-chain, we examined the mTEC presentation of two C-peptide epitopes, CP1 and CP2, which are encoded by the *Ins1* and *Ins2* genes, respectively. CP1 (GDLQTLALEVARQ) and CP2 (GDLQTLA-LEVAQQ) originate from the C-terminus of C-peptide and have a single residue difference in the MHC-II-binding core (underlined)³¹. We used non-cross-reactive CD4⁺ T cell hybridomas specific for CP1 or CP2 (Supplementary Fig. 4c) and found that mTECs spontaneously presented CP2, whereas presentation of CP1 was similar to the background (Fig. 3d). These results are consistent with the selective expression of the *Ins2* gene in mouse thymus. This genetic difference also resulted in the selective presentation of the CP2 epitope in the thymus.

Next, we extended the presentation analysis to other thymic APCs purified from 3 to 6-week-old NOD mice, including type 1 and type 2 conventional dendritic cells (cDC1 and cDC2, respectively), B cells, and a B220⁺CD11c⁺ population containing plasmacytoid DCs (pDCs) and CD11c⁺ B cells (Supplementary Fig. 4d). We observed consistent presentation of E21 from cDC2 but not from other populations. cDC1 occasionally presented E21, but the overall responses were insignificant (Fig. 3e). The presentation of E21 was epitope-specific, as it was not detected in any of the thymic APC subsets from NOD.B16A mice (Fig. 3e). In contrast to E21, presentation of G20 was at the background level in all the thymic APCs from WT NOD mice (Fig. 3e).

The results indicating restricted thymic insulin presentation led us to determine whether insulin epitope presentation is more diversified in pancreatic islets due to the presence of the tissue-intrinsic crinophagic pathway. First, we examined spontaneous presentation of G20, E21, CP1, and CP2 in dispersed islet cells isolated from 3 to 4-week-old female NOD or NOD.B16A mice (Fig. 3f). In contrast to the thymus, we observed similar levels of presentation for both G20 and E21 in islets isolated from NOD mice (Fig. 3g). Notably, this presentation was epitope-specific, as dispersed islets from NOD.B16A mice did not present either epitope (Fig. 3g). Also, in line with the expression of both *Ins1* and *Ins2* in pancreatic islets, we detected presentation of both CP1 and CP2 (Fig. 3h).

Next, we evaluated different islet APCs purified from infiltrated islets from 8 to 10-week-old female mice, including the resident macrophages and islet-infiltrating cDC1 and cDC2 (Supplementary Fig. 4e). We detected spontaneous presentation of both G20 and E21 in all of these islet APCs from NOD mice but not in islet macrophages sourced from NOD.B16A mice (Fig. 3i).

Lastly, when we pulsed dispersed islets from 8 to 10-week-old female NOD mice with intact insulin, we found that only presentation of E21, but not G20, was enhanced (Fig. 3j). However, exogenous pulse with the free B:9–23 peptide increased presentation of both epitopes (Fig. 3j). These results suggest that the discrepancy in epitope presentation between the thymus and islets is not due to an intrinsic difference in APCs. In summary, we found a clear difference in insulin epitope presentation between the thymus and the islets. The pathogenic role of crinophagy is corroborated by results showing that the immunogenic G20 epitope derived from crinosomes is mostly undetectable in the thymus.

The thymic epitope repertoire is broad but constrained

The crinosome peptidome contained a wide range of β -cell-derived peptides that were diminished by chloroquine treatment. Given the constrained insulin presentation in the thymus and that crinophagy is an inherent feature in endocrine tissues, we were prompted to broadly investigate the distinct characteristics of the thymic MHC-II peptidome, where the crinophagic pathway is unlikely to operate. In particular, we aimed to unbiasedly identify β -cell-derived, MHC-II-bound

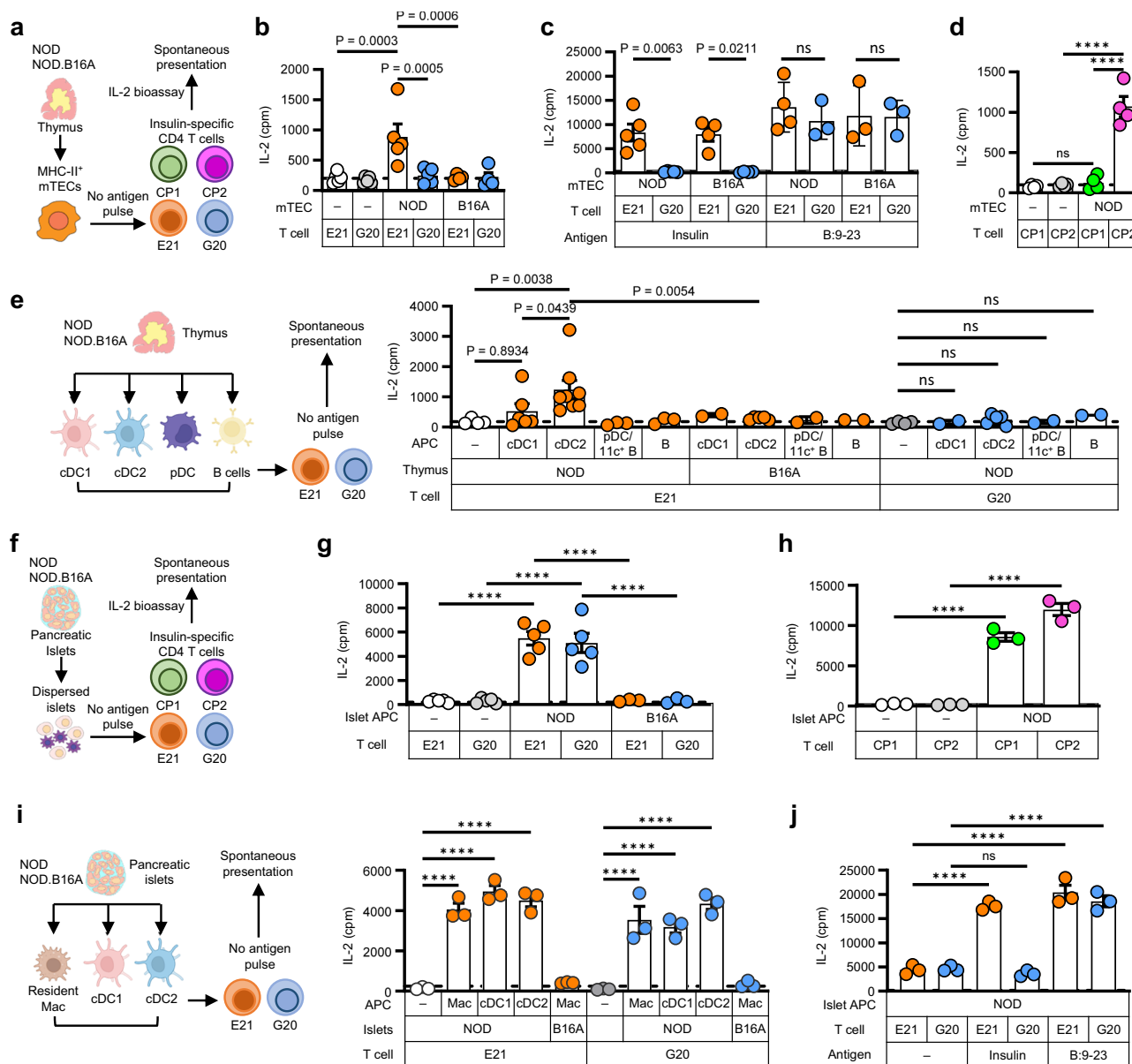


Fig. 3 | Thymus and pancreatic islets present different insulin epitopes.

a Schematic of an antigen presentation assay to probe the spontaneous presentation of four insulin epitopes by MHC-II-expressing mTECs. Created in BioRender. Wan, X. (2024) BioRender.com/s20b261. **b** Spontaneous presentation of G20 and E21 by MHC-II⁺ mTECs. For NOD mice, $n = 25$ in 5 independent experiments; for NOD.B16A mice, $n = 18$ in 4 independent experiments. **c** Presentation of G20 and E21 by MHC-II⁺ mTECs during pulse with intact insulin (10 μ M) or B:9-23 peptide (1 μ M). For NOD mice with insulin pulse, $n = 25$ in 5 independent experiments; for NOD mice with B:9-23 pulse, $n = 20$ in 4 independent experiments; for NOD.B16A mice with insulin pulse, $n = 18$ in 4 independent experiments; for NOD.B16A mice with B:9-23 pulse, $n = 12$ in 3 independent experiments. **d** Spontaneous presentation of CP1 and CP2 by MHC-II⁺ mTECs, $n = 20$ in 4 independent experiments. **e** Spontaneous presentation of G20 and E21 by various thymic APCs. For NOD mice examined for the E21 response: $n = 9$ in 3 independent experiments for B-cell and pDC presentation; $n = 20$ for cDC1 and cDC2 presentation in 5 and 8 independent experiments, respectively (due to the higher abundance of cDC2, the 20 mice were separated into 8 independent experiments). For NOD.B16A mice examined for the E21 response: $n = 6$ in 2 independent experiments, except for cDC2, where the cells

were abundant enough for 5 independent experiments. For NOD mice examined for the G20 response: $n = 6$ in 2 independent experiments, except for cDC2, where the cells were abundant enough for 5 independent experiments. A schematic figure is created in BioRender. Wan, X. (2024) BioRender.com/s20b261 **f** Schematic for assessing the spontaneous presentation of four proinsulin epitopes in dispersed islet cells, created in BioRender. Wan, X. (2024) BioRender.com/s20b261. **g** Spontaneous presentation of G20 and E21 by dispersed islet cells: $n = 15$ for NOD mice in 5 independent experiments, and $n = 9$ for NOD.B16A mice in 3 independent experiments. **h** Spontaneous presentation of CP1 and CP2 by dispersed islet cells, $n = 9$ in 3 independent experiments. **i** Spontaneous presentation of G20 and E21 by different APCs purified from pancreatic islets, $n = 15$ in 3 independent experiments. A schematic figure is created in BioRender. Wan, X. (2024) BioRender.com/s20b261. **j** Presentation of G20 and E21 by dispersed islet cells during pulse with intact insulin (10 μ M) or B:9-23 peptide (1 μ M), $n = 15$ in 3 independent experiments. In all experiments, the data summarize results (mean \pm s.e.m) pooled from multiple independent experiments, with each symbol representing one experiment. Each experiment included APCs sourced from 3 to 8 mice per strain. ns not significant; **** $P < 0.0001$. One-way ANOVA with Sidak's multiple comparisons test.

epitopes that are naturally presented in the thymus, to facilitate further analysis of their corresponding CD4⁺ T cells.

In a previous study, we performed an MHC-II immunopeptidome analysis using pancreatic islets isolated from 219 NOD mice, where we

identified diverse MHC-II-bound peptides from β -cell proteins, such as insulin, ChgA, IAPP, SCG, vitamin D-binding protein (DBP), and ZnT8³¹. Notably, these tissue-derived peptides only constituted a minor fraction of the islet peptidome relative to the dominant peptides that are

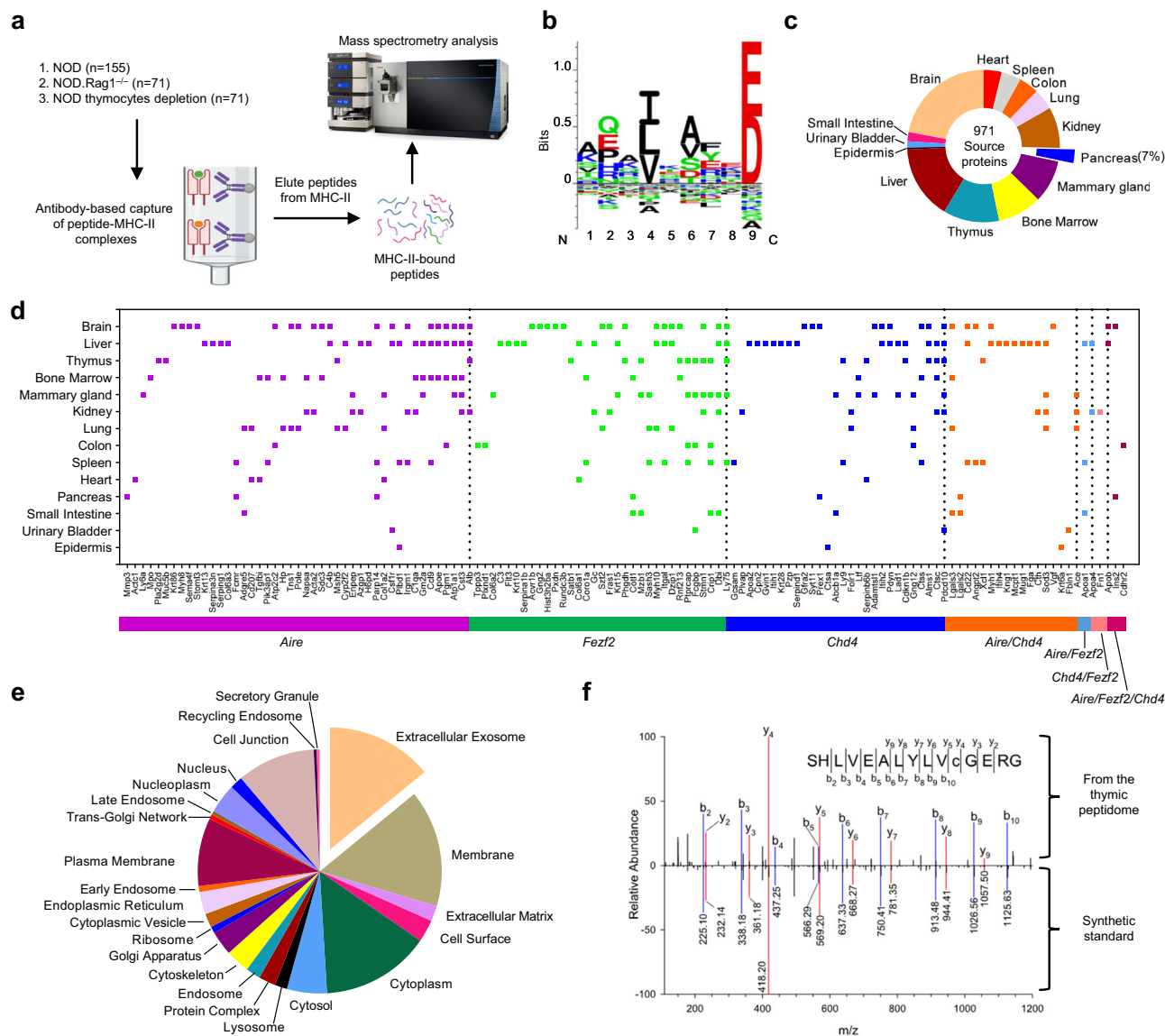


Fig. 4 | Thymic immunopeptidome analysis reveals a broad MHC-II epitope repertoire containing a minor component of islet-derived epitopes.

a Schematic for three independent analyses of the thymic MHC-II peptide, created in BioRender. Wan, X. (2024) BioRender.com/s20b261. **b** Gibbs cluster analysis of all the identified thymic MHC-II peptides showing an I-A^{E7}-binding motif. **c** Tissue localization analysis of the source proteins of the identified thymic MHC-II peptides. **d** Illustration of a fraction of PTAs that were mapped to different

peripheral tissues (y-axis), which also corresponded to genes known to be regulated by Aire, Fezf2, and Chd4 (x-axis). **e** Cellular component analysis of the source proteins of the identified peptides in the thymic MHC-II peptide. The pie chart depicts the protein counts of indicated cellular components. **f** A mirror plot depicts a complete match of the identified B:9–23 sequence (with cysteine oxidized to cysteic acid) via antibody capture in the thymic MHC-II peptide (upper) with its synthetic standard (lower).

ubiquitously expressed (i.e., actin). Given that the thymus is a highly complex tissue with few MHC-II-expressing APCs, we anticipated that identifying β -cell-derived peptides would be highly challenging. Therefore, we performed three independent analyses to investigate the thymic MHC-II peptidome (Fig. 4a). Initially, we accumulated thymic cells collected from 155 WT NOD mice in which thymocytes were partially removed through gentle agitation. To further enrich thymic APCs, we repeated the analysis using 71 NOD.*Rag1*^{-/-} mice or 71 NOD mice subjected to further removal of thymocytes by magnetic depletion. In all three experiments, the frozen cell pellets were lysed, followed by antibody-based isolation of the peptide-MHC-II complexes. The peptides were then eluted from the MHC-II molecules and analyzed by mass spectrometry (Fig. 4a).

Our analysis revealed several general signatures of the thymic MHC-II peptidome. Reflecting typical features of MHC-II-bound

peptides, the identified sequences from the three analyses clustered into peptide families, characterized by different lengths but originating from the same protein region (Supplementary Data 1). Gibbs cluster analysis of all the peptides from the three experiments (4305 peptides from 1403 families; Supplementary Data 2) converged into a single cluster with a strong preference for an acidic residue at P9 (Fig. 4b). This signature was consistent with previously defined I-A^{E7}-binding motifs^{31,58}, confirming the specificity of the thymic MHC-II peptidome.

We assessed tissue localization of the source proteins of the identified MHC-II peptides using the DAVID (Database for Annotation, Visualization and Integrated Discovery) tool⁵⁹. A vast majority of the source proteins (971 out of 1076; 90%) were mapped to single or multiple peripheral tissues (FDR < 0.05), including the brain, liver, intestine, heart, and pancreas (Supplementary Fig. 5a, Fig. 4c and

Supplementary Data 3), indicating their identity as peripheral-tissue antigens (PTAs). A fraction of these PTAs corresponded to transcripts that showed a significant reduction in mTECs isolated from C57BL/6 mice lacking *Aire*, *Fezf2*, or *Chd4* (Fig. 4d and Supplementary Data 4), transcriptional regulators known to drive PTA expression^{60–63}. These data underscore the diversity of MHC-II epitopes presented in the thymus as a reflection of the promiscuous gene expression by mTECs.

By cellular component analysis, we found that a notable fraction of the identified PTAs were associated with extracellular exosomes (Supplementary Fig. 5b and Fig. 4e), which are involved in antigen transfer in the thymus⁶⁴. We then overlaid our peptidome data with recent single-cell RNA sequencing (scRNA-seq) analysis of post-*Aire* mTECs displaying intermediate to low levels of MHC-II expression (MHC-II^{lo})⁶⁵. This MHC-II^{lo} mTEC population consisted of distinct subtypes that exhibited transcriptional similarities to various peripheral cell types, including microfold, tuft, muscle, goblet, and neuroendocrine cells⁶⁵. We found 222 source proteins that corresponded to signature marker genes expressed by these mimetic mTEC subtypes (Supplementary Fig. 5c). These findings suggest that these PTAs might be expressed by MHC-II^{lo} mTECs and then acquired and presented by MHC-II-expressing APCs in the thymus.

After characterizing the global thymic MHC-II peptidome, we focused on whether β -cell-derived epitopes could be identified. First, we analyzed peptides that were mapped to the whole pancreas, which only constituted a small fraction of the thymic peptidome (Fig. 4c). Most of these peptides originated from proteins expressed in the exocrine pancreas (not depicted), in line with the fact that the exocrine tissue makes up >95% of the pancreas volume. By analyzing peptides from the endocrine islets, we identified several peptide families belonging to β cells, including insulin-2 C-peptide, ChgA, DBP, and ZnT8 (Supplementary Data 1). Notably, all these peptide families were previously identified in the MHC-II peptidome of pancreatic islets³¹. Second, reflecting the limited sensitivity of the direct immunopeptidome analysis for identifying certain low-abundance peptides, we did not detect peptides from the insulin B-chain. Considering that insulin B-chain contains two cysteine residues that are susceptible to oxidation, which may hinder their detection in highly complex samples⁶⁶, we developed an antibody capture method to enrich these peptides from the thymic peptidome (Supplementary Fig. 5d). Specifically, we incubated the entire thymic MHC-II peptide pool with a mixture of two monoclonal antibodies that complementarily recognize different peptide segments spanning the entire insulin B-chain (Supplementary Fig. 5e). Analysis of the peptides captured by the antibodies showed a sequence of B:9–23 with oxidized cysteine to cysteic acid, which was verified by showing a complete match to the synthetic standard (Fig. 4f). These results provided chemical evidence that the long B:9–23 peptide as an MHC-II-bound sequence presented in the thymus. Third, we exhaustively searched the thymic peptidome for the presence of HIPs and deamidated C-peptides. The results indicated that these modified peptides were below the detection threshold, supporting the notion that thymus generally lacks the presentation of post-translationally modified antigens^{67,68}. In summary, our immunopeptidome analysis documented the broad spectrum of thymic epitope presentation encompassing a wide range of peripheral tissues. However, in the context of T1D, the scope of the thymic epitope repertoire may still be insufficient to tolerate a group of unconventional epitopes provided by crinophagy.

CD4⁺ T cells to unconventional insulin epitopes are transcriptionally distinct

Our antigen presentation and immunopeptidome analysis suggested that the thymus largely lacked the presentation of unconventional insulin epitopes generated in crinosomes. Because thymic epitopes are low in abundance and the MHC-II peptidome analysis is limited in sensitivity, we could not conclusively determine the absolute absence

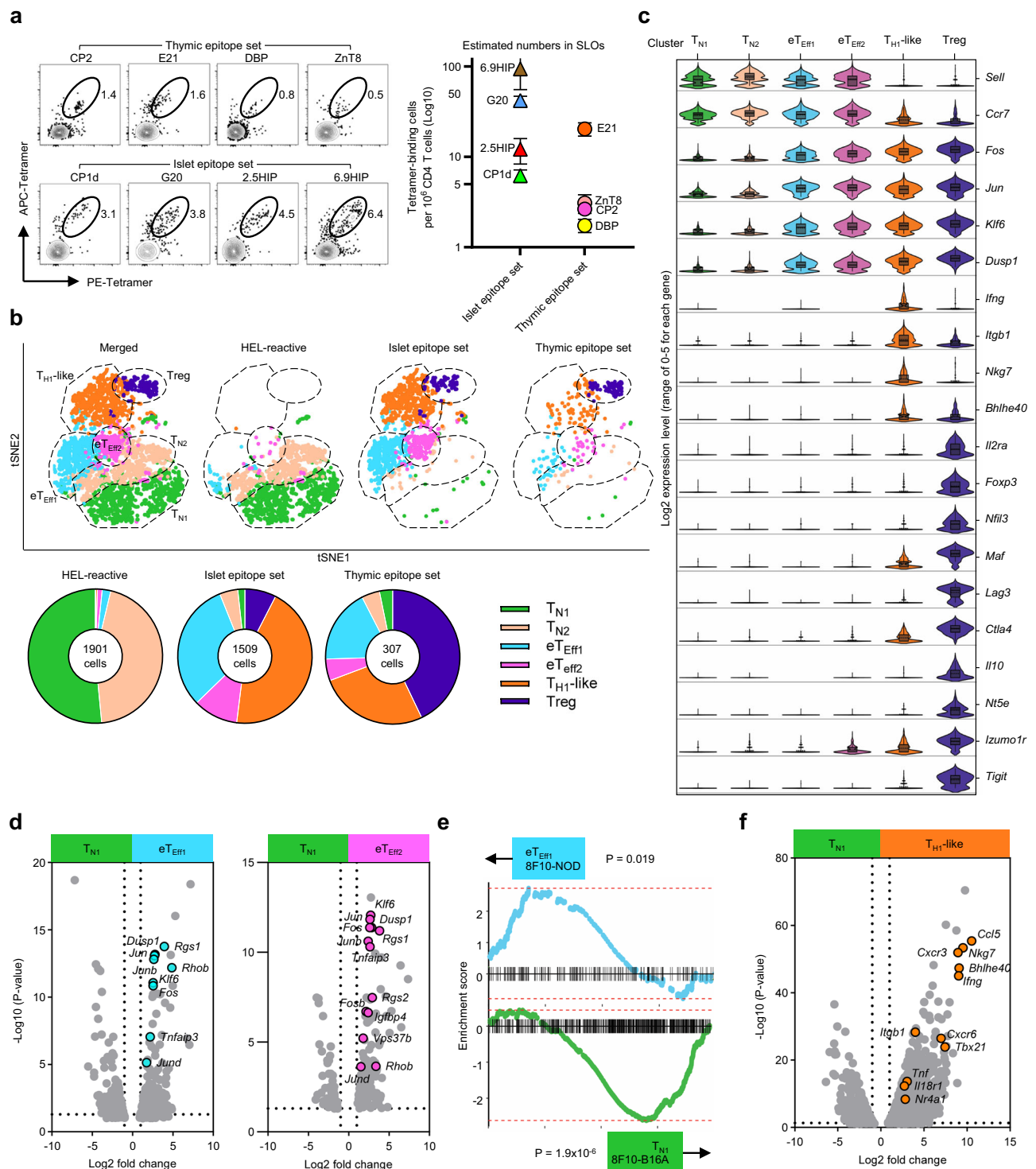
of crinosome-derived epitopes in the thymus. To address this caveat, we decided to investigate CD4⁺ T cells corresponding to epitopes that are differentially presented between thymus versus pancreatic islets. Our hypothesis was that if crinosome-derived epitopes, such as G20, deamidated C-peptide, and HIPs, are minimally presented in the thymus, their corresponding CD4⁺ T cells would manifest an autoreactive phenotype. On the other hand, CD4⁺ T cells reactive to epitopes that were indicated to be presented in the thymus, such as E21, CP2, DBP, and ZnT8, should be tolerized.

We developed I-A^{g7}-based tetramers incorporating a group of unconventional insulin-derived epitopes, including G20, a deamidated CP1 epitope (CP1d), and two HIPs (2.5HIP and 6.9HIP), referred to as islet epitope set. CP1d corresponds to the native CP1 epitope having a Q-to-E conversion (GDLQTLALEVARQ → GDLQTLALEVARE), a modification that enhanced the binding affinity to I-A^{g7}³¹. 2.5HIP and 6.9HIP are formed by a shared C-peptide segment (LQTLAL) with segments of ChgA (WSRMD) and IAPP (NAARD), respectively, making them strong agonists to CD4⁺ T cell clones BDC2.5 and BDC6.9^{47–49}. In parallel, we also produced tetramers containing E21, CP2, DBP, and ZnT8, referred to as thymic epitope sets (Supplementary Fig. 6a and 6b). All the tetramers used identical epitope sequences to those indicated by antigen presentation and immunopeptidome analysis (Supplementary Fig. 7a).

We used a cell-based competitive binding assay to evaluate the relative binding affinities of each individual epitope to I-A^{g7}. Although the individual epitopes exhibited variations in their binding affinities, the overall binding between the thymic and islet epitope sets was similar (Supplementary Fig. 7b). Considering the highly similar sequences between G20 and E21, we tested in vitro T cell stimulation using plate-bound G20:I-A^{g7} and E21:I-A^{g7} monomers. Both monomers activated their cognate CD4⁺ T cell hybridomas without causing crossreactivity (Supplementary Fig. 7c). Using the magnetic enrichment protocol⁶⁹, we detected tetramer-binding CD4⁺ T cells for each epitope in SLO (Fig. 5a) and thymus (Supplementary Fig. 7d) of 6–8-week-old female NOD mice. Minimal tetramer binding was observed in CD8 T cells at both sites (Supplementary Fig. 7e). We also estimated the numbers of tetramer-binding CD4⁺ T cells for each epitope using a fluorescent beads-based counting method⁶⁹. In SLOs, the T cells specific to the islet epitopes ranged from 10 to 100 per million CD4⁺ T cells (Fig. 5a). In contrast, we observed a low number of T cells specific to three thymic epitopes (CP2, DBP, ZnT8; less than 5 tetramer-binding cells per million CD4⁺ T cells), except for E21-reactive T cells (Fig. 5a). This profile correlated with numbers measured in single-positive CD4⁺ Thymocytes, where the majority of T cells responding to thymic epitopes showed low numbers (Supplementary Fig. 7d).

We performed scRNA-seq analysis on CD4⁺ T cells using a combination of tetramers containing either thymic (CP2, E21, DBP, ZnT8) or islet (CP1d, G20, 2.5HIP, 6.9HIP) epitopes. Naïve TCR transgenic CD4⁺ T cells (CD4⁺CD25[−]CD69[−]CD44^{hi}CD62L^{hi}) specific for the I-A^{g7}-binding hen egg lysozyme (HEL) 11–25 peptide were included as a control. We FACS-sorted the three T cell populations from SLOs of 6–8-week-old female mice, barcoded them using cell hashing reagents, and performed multiplexed scRNA-seq analysis in replicates.

We identified six distinct cell clusters among the three T cell populations (Fig. 5b). As expected, HEL-reactive T cells were found in two clusters representing naïve CD4⁺ T cells (T_{N1} and T_{N2}) (Fig. 5b). Both clusters expressed typical naïve T cell markers, including *Sell*, *Ccr7*, and *Satb1* (Fig. 5c). T_{N2} exhibited higher expression of *Cd5* and *Cd6* compared to T_{N1} (Supplementary Fig. 8a), suggesting ongoing tonic signaling. Tetramer-binding CD4⁺ T cells specific to the thymic epitopes were highly represented in a cluster indicative of regulatory T cells (Treg) (Fig. 5b). This cluster showed high expression of Treg lineage genes, including surface markers *Il2ra*, *Tnfrsf18*, *Lamc1*, and transcription factors *Foxp3*, *Maf*, *Ikzf2*, *Nfil3* (Fig. 5c and Supplementary Fig. 8b). Moreover, we found that a set of genes related to inhibitory functions, such as *Lag3*, *Ctla4*, *Il10*, *Nt5e* (encoding CD73),



Izumo1r (encoding FR4), and *Tigit*, were predominantly expressed within the Treg cluster (Fig. 5c and Supplementary Fig. 8b). Thus, at the transcriptional level, the CD4⁺ T cells reactive to thymic epitopes manifested a tolerant phenotype.

In stark contrast, almost all the tetramer-binding T cells in the islet epitope group were in three clusters at different stages of activation, including early effectors (eT_{Eff1} and eT_{Eff2}) and further differentiated T_{H1}-like cells (Fig. 5b). eT_{Eff1} and eT_{Eff2} retained some naïve markers but upregulated genes associated with NF-κB activation (*Fos*, *Jun*, *Dusp1*, *Klf6*, *Tnfrsf3*, *Zfp36*) (Fig. 5c and d). eT_{Eff2} showed increased expression of *Cd69*, *Igf1p4*, and *Vps37b* compared to eT_{Eff1} (Supplementary

Fig. 8c), suggesting a relatively higher activation state. These early effectors were reminiscent of a G20-specific TCR transgenic T cell (8F10) that manifested intermediate priming upon weak but continuous interactions with insulin peptides presented in distant lymph nodes²⁸. This observation was further supported by gene set enrichment analysis (GSEA), which revealed significant enrichment of highly differentially expressed genes (DEGs) in the eT_{Eff1} cluster that was upregulated in 8F10 T cells sourced from inguinal lymph nodes of NOD (antigen-replete) versus NOD.B16A (antigen-deleted) mice (Fig. 5e). Thus, although the early activation signature may result from artificial tetramer engagement, it also mirrored a previously observed in vivo

Fig. 5 | scRNA-seq analysis reveals distinct signatures in CD4⁺ T cells specific for epitopes presented in the thymus versus pancreatic islets. **a** Tetramer-binding CD4⁺ T cells for indicated epitopes in SLOs of 6–8-week-old female NOD mice. The FACS plots depict double-positive tetramer-binding populations (gated on CD45⁺B220⁺CD8⁺CD11b⁺A^β7-Thy1.2⁺CD4⁺) in cells with magnetic enrichment. The dot plot shows the numbers of tetramer-binding T cells for each epitope (mean ± s.e.m) quantified from 4 to 8 individual mice in four independent experiments ($n = 4$: 2.5HIP, $n = 4$: 6.9HIP, $n = 4$: CP1d, $n = 8$: G20, $n = 7$: E21, $n = 4$: CP2, $n = 4$: DBP, $n = 4$: ZnT8). **b** tSNE plots (upper) showing cellular heterogeneity of indicated T cell populations. The pie charts (lower) depict the composition of different transcriptional clusters in the three T cell populations. The data are merged from two independent scRNA-seq analyses of tetramer-binding CD4⁺ T cells sourced from SLOs of 6–8-week-old female NOD mice. T cells for the thymic and islet epitope set were sorted from 24 and 10 mice included in two independent experiments, respectively. **c** Violin plots depicting function-related genes that were differentially

expressed among CD4⁺ T cell clusters (Benjamini–Hochberg correction for multiple tests). For each gene, the Log2 expression level range is 0–5. **d** Signature genes that were upregulated in the two early effector clusters compared to the naïve T cell cluster. All the genes described in this Figure meet the statistical cut-off (adjusted $P < 0.05$) using the Benjamini–Hochberg correction for multiple tests. **e** GSEA analysis of the early effector and naïve T cell clusters identified in this study using a previous dataset depicting intermediate priming of a G20-specific TCR transgenic T cell (8F10) sourced from inguinal lymph nodes of WT NOD or NOD.B16A mice. The weighted Kolmogorov–Smirnov statistic was performed. The data show that genes upregulated in the early effector cluster were significantly enriched for genes upregulated in 8F10 T cells from the antigen-replete NOD condition, whereas the naïve T cell cluster resembled 8F10 T cells sourced from the antigen-deplete NOD.B16A condition. **f** Signature genes representing the T_H1-like cluster as compared to the naïve cluster, based on nonparametric Wilcoxon rank sum test with Benjamini–Hochberg correction for multiple testing.

signature. About half of the T cells in the islet epitope group were classified into the T_H1-like cluster (Fig. 5b), which exhibited sustained expression of NF- κ B activation genes and upregulated genes signifying T_H1 differentiation, such as *Ifng*, *Itgb1*, *Nkg7*, *Cxcr3*, *Bhlhe40*, and *Tbx21* (Fig. 5c, f). Thus, at the transcriptional level, CD4⁺ T cells in the islet epitope set exhibited a distinctive phenotype associated with activation and pathogenicity.

Crinosome-derived insulin epitopes elicit autoreactive T-cell responses

Our transcriptional results support that crinosomes can provide unique epitopes for recognition by CD4⁺ T cells escaping tolerance. To strengthen these results, we performed flow cytometry analysis of tetramer-binding CD4⁺ T cells reactive to individual thymic or islet epitopes (Supplementary Fig. 6c, d). About 60–70% of CD4⁺ T cells specific to each thymic epitope were FOXP3⁺ Tregs in SLOs (Fig. 6a). This profile was distinct in each T cell of the islet epitope group, where only 10–15% were FOXP3⁺ Tregs, a level similar to tetramer-negative polyclonal CD4⁺ T cells (Fig. 6a). In addition to SLOs, we found that a majority of the E21-reactive CD4⁺ single-positive thymocytes were also FOXP3⁺ Tregs, whereas G20-reactive cells were mostly FOXP3[−] conventional T cells (Fig. 6b). Thus, while CD4⁺ T cells to the thymic epitopes are successfully converted into Tregs, this tolerance mechanism is largely missing in T cells reactive to the unconventional islet epitopes.

In addition to the FOXP3⁺ Treg population, we noticed a FOXP3[−]CD44^{hi} subset within each of the tetramer-binding CD4⁺ T cells specific to the islet epitopes, indicating their antigen experienced status in the periphery (Fig. 6a). This FOXP3[−]CD44^{hi} subset was also found in the T cells reactive to the thymic epitopes CP2 and E21 (Fig. 6a). For further characterization, we assessed the expression of CD73 and FR4, two markers associated with T-cell anergy⁷⁰, in the FOXP3⁺ (Treg), FOXP3[−]CD44[−] (naïve T cells) and FOXP3[−]CD44^{hi} subsets (Supplementary Fig. 6e). Aligning with our single-cell RNAseq analysis, the FOXP3⁺ Treg subset in T cells recognizing either the thymic (E21) or islet (G20, 2.5HIP, 6.9HIP) epitopes showed high expression of both CD73 and FR4, whereas the FOXP3[−]CD44[−] naïve T cells showed minimal expression (Supplementary Fig. 9a). Notably, we found high expression of both CD73 and FR4 in the FOXP3[−]CD44^{hi} subset in E21:I-A^β7 tetramer-binding T cells, indicating an anergic phenotype (Supplementary Fig. 9a). However, the FOXP3[−]CD44^{hi} population in the three T cells for the islet epitopes (G20, 2.5HIP, and 6.9HIP) showed much less expression of CD73 and FR4 (Supplementary Fig. 9a), supporting an effector phenotype. Thus, T-cell anergy, an important peripheral tolerance mechanism, is also limited in CD4⁺ T cells to the unconventional islet epitopes.

To confirm these results functionally, we immunized NOD mice with B:9–23 and assessed T cell responses (IFN γ production) upon recall with Syn-G20 or Syn-E21. In contrast to robust responses from

Syn-G20, minimal responses to Syn-E21 were detected in individual NOD mice upon immunization (Fig. 6c), indicating that the G20 but not the E21 epitope confers immunogenicity. However, treating NOD mice with monoclonal antibodies that disturb Treg functions, including anti-TGF β , anti-CTLA4, and anti-CD25, consistently reversed the unresponsiveness of the E21-reactive T cells (Fig. 6c). This analysis was then extended to all the islet and thymic epitopes in vivo without immunizing with exogenous peptides. Specifically, we isolated total cells pooled from pancreatic draining lymph nodes (pLN) and islets from 8–10-week-old female NOD mice and stimulated them with each epitope individually in the presence of low-dose IL-2. We stimulated the cells for two 7-day cycles (total 14 days), which was shown to detect epitope-specific response³¹. Each islet epitope was able to induce detectable IFN γ production, as assayed by ELISPOT, whereas the responses to all the thymic epitopes were mostly negative (Fig. 6d). Moreover, we treated NOD mice with the anti-CD25 antibody and assessed T cell responses post the two-cycle stimulation with each of the thymic epitopes in cells from islets and pLN. Notably, responses to all four thymic epitopes became detectable in mice with treatment with anti-CD25 antibody (Fig. 6e). These results demonstrated that while CD4⁺ T cells in the thymic epitope set are maintained at a dormant state due to Treg control, those recognizing the unconventional islet epitopes are readily responsive to antigen stimulation.

Our analysis indicates that the lack of the crinosome-derived G20 epitope in the thymus is tightly linked to the autoimmune phenotypes observed in its cognate T cells. To strengthen this finding, we explored whether ablating thymic presentation of the conventional E21 epitope would transform this specificity to autoreactive T cells. Given that E21 derives processing of intact insulin, we utilized NOD mice deficient with the *Ins2* gene (NOD.*Ins2*^{−/−}). This strain lacks insulin expression in the thymus but shows normal systemic insulin levels and, notably, exhibited accelerated diabetes development (ref. 17,71; Supplementary Fig. 9b). The numbers of both G20- and E21-tetramer-binding CD4⁺ T cells were comparable in SLOs between 6-week-old female NOD and NOD.*Ins2*^{−/−} mice (Supplementary Fig. 9c). However, *Ins2* deficiency substantially impaired Treg differentiation of E21-specific CD4⁺ T cells in both the thymus (Fig. 7a) and SLOs (Fig. 7b), whereas the peripheral G20-reactive T cells were not significantly affected (Fig. 7b), confirming that the natural expression of insulin in the thymus precisely and selectively governs Treg differentiation of the E21-specific T cells. Additionally, we found that the FOXP3[−]CD44^{hi} E21-specific T cells in SLOs of NOD.*Ins2*^{−/−} mice retained a high expression level of CD73 and FR4 (Supplementary Fig. 9d), suggesting that the energy phenotype was not mediated by thymic insulin presentation but mainly occurred in the periphery. Thus, when thymic E21 presentation is deleted genetically, the E21-specific CD4⁺ T cells exhibit a conventional T cell phenotype, resembling those reactive to the G20 epitope at the steady state.

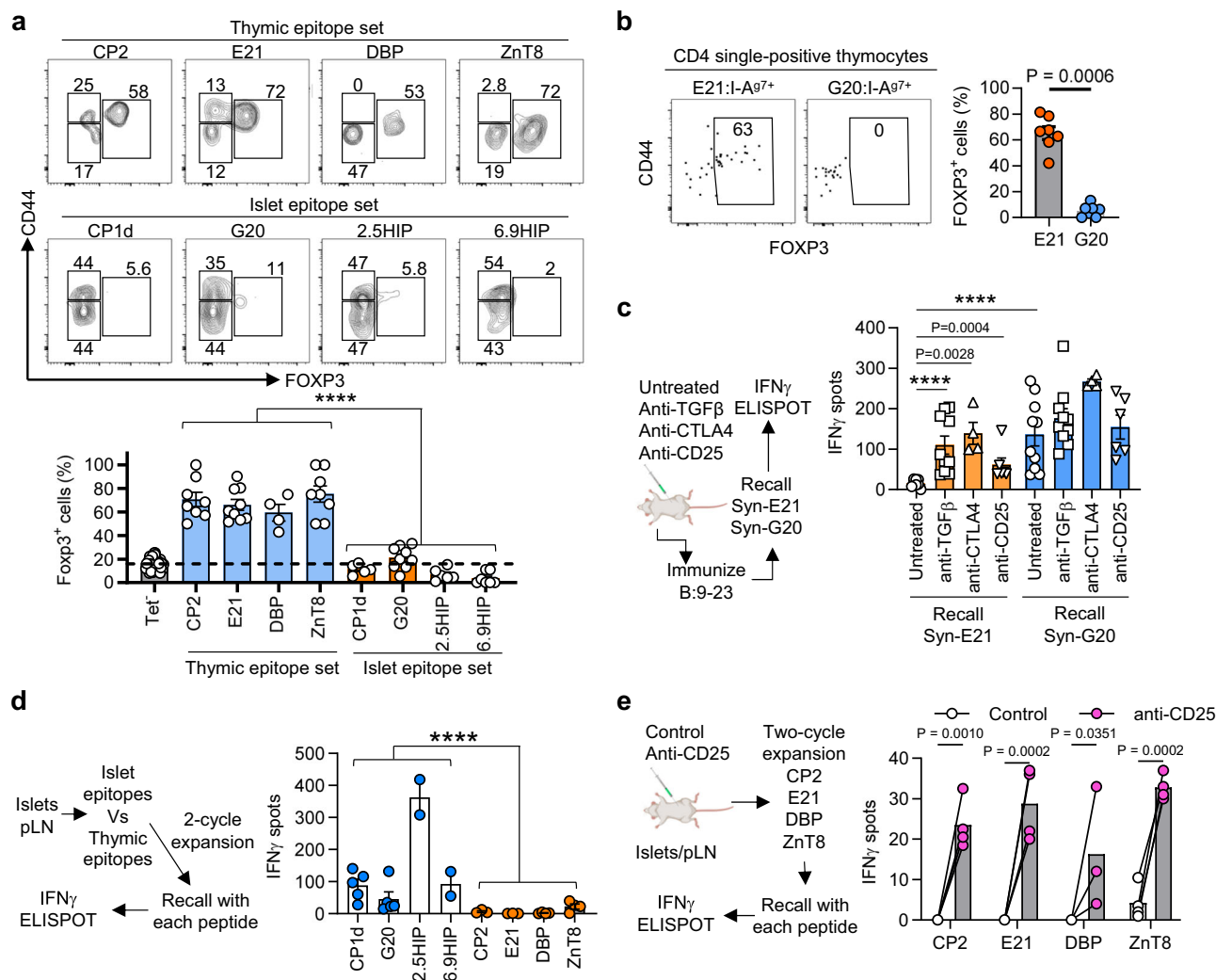


Fig. 6 | CD4⁺ T cells reactive to unconventional epitopes derived from crinomes exhibit a nontolerant phenotype associated with pathogenicity. **a** Flow cytometry analysis of peripheral tetramer-binding CD4⁺ T cells for expression of FOXP3 and CD44. The quantification (right) summarizes the percentage of the FOXP3⁺ Treg population in tetramer-positive epitope-specific and tetramer-negative (Tet⁻) polyclonal CD4⁺ T cells. Data (mean \pm s.e.m) summarize results from 4 to 6 independent experiments; each symbol represents results from an individual mouse ($n=8$: CP2, $n=9$: E21, $n=4$: DBP, $n=8$: ZnT8, $n=5$: CP1d, $n=9$: G20, $n=6$: 2.5HIP, $n=7$: 6.9HIP, $n=37$: polyclonal T cells). **** $P < 0.0001$; Two-way ANOVA analysis. **b** Flow cytometry analysis of FOXP3⁺ Tregs in E21:I-A^{g7+} and G20:I-A^{g7+} tetramer-binding CD4⁺ single-positive thymocytes. The bar graph quantifies the percentage of FOXP3⁺ cells among the tetramer-binding CD4⁺ T cells. Data (mean \pm s.e.m) summarize results from three independent experiments; each symbol represents results from an individual mouse ($n=7$). *** $P = 0.0006$; Mann-Whitney test, two-tailed. **c** ELISPOT assay for assessing T cell responses upon recall with Syn-E21 (TEGEALYLVCGE) or Syn-G20 (TEGVEALYLVCGE) in NOD treated with different blocking antibodies and immunized with the B:9-23 peptide ($n=10$ for untreated group, $n=10$ for anti-TGF β treated group, $n=4$ for anti-CTLA4 treated group, $n=6$ for anti-CD25 treated group). Data (mean \pm s.e.m) summarize results from three independent experiments; each symbol represents results from

an individual mouse. ** $P = 0.0028$; *** $P = 0.0004$; **** $P < 0.0001$; Mann-Whitney test, two-tailed. The schematic figure is created in BioRender. Wan, X. (2024) BioRender.com/y60m085. **d** ELISPOT assay for assessing T cell responses upon recall with each individual epitope in the thymic or islet epitope set after a two-cycle in vitro stimulation of islets and pLN cells with the same peptides. Data (mean \pm s.e.m) summarize results from 2 to 5 independent experiments; each symbol represents a biological replicate including 4–6 mice pooled together. ($n=20$ for CP1d and G20 in 5 independent experiments, $n=8$ for 2.5HIP and 6.9HIP in 2 independent experiments, $n=18$ for CP2 and E21 in 3 independent experiments, $n=20$ for DBP and ZnT8 in 4 independent experiments) **** $P < 0.0001$; Two-way ANOVA analysis. **e** ELISPOT assay for assessing T cell responses upon recall with each individual thymic epitope after a two-cycle in vitro stimulation of islets and pLN cells pooled from NOD mice treated with the control or the anti-CD25 antibody. Data (mean \pm s.e.m) summarize results from multiple independent experiments; each symbol represents a biological replicate including 4–6 mice pooled together. ($n=20$ for CP2, E21, and ZnT8 in 4 independent experiments; $n=16$ for DBP in 3 independent experiments). * $P = 0.0351$; ** $P = 0.001$; *** $P = 0.0002$; Repeated measures two-way ANOVA with Bonferroni's multiple comparisons test. The schematic figure is created in BioRender. Wan, X. (2024) BioRender.com/s30d279.

To further test the functionality of the E21-reactive T cells, we immunized NOD and NOD.*Ins2*^{-/-} mice with B:9-23 and tested T cell responses upon recall with two antigens that give rise to the E21 epitope: intact insulin and Syn-E21 (Fig. 7c). Responses to either antigen were minimal in WT NOD mice but were significantly enhanced in NOD.*Ins2*^{-/-} mice (Fig. 7c). Thus, E21-specific

T cells switch to an autoreactive phenotype when thymic insulin presentation is absent. Overall, our studies indicate that crinophagy diversifies the epitope repertoire in pancreatic islets that extends beyond thymic control, linking this physiological pathway to its pathological role in the development of autoimmune diabetes.

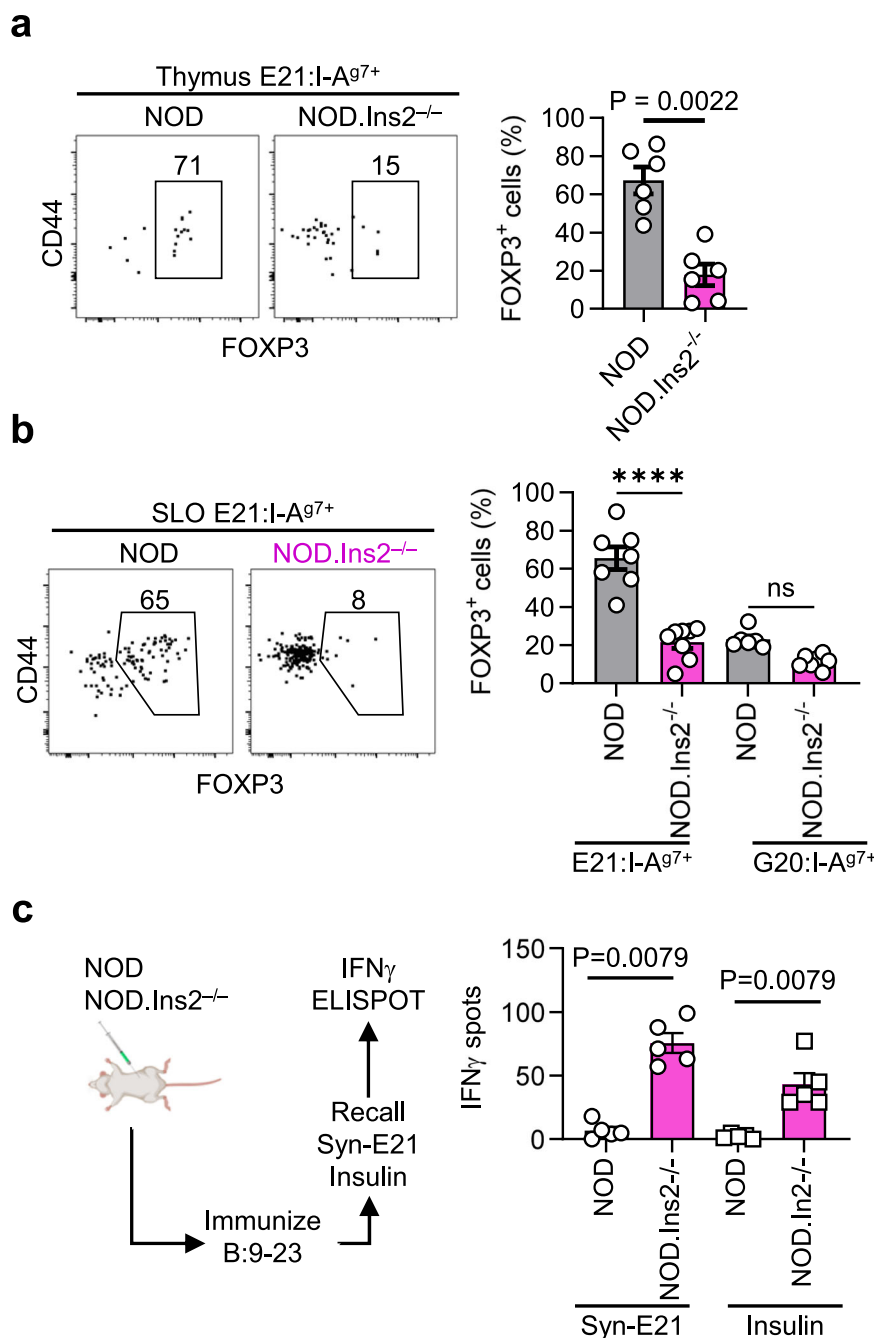


Fig. 7 | E21-specific T cells derived from NOD.Ins2^{-/-} mice exhibit a nontolerant phenotype. a Flow cytometry analysis of FOXP3⁺ Tregs in E21:I-A^{g7} tetramer-binding CD4⁺ T cells in the thymus of 6-week-old female NOD and NOD.Ins2^{-/-} mice. Data (mean ± s.e.m) summarize results from three independent experiments; each symbol represents results from an individual mouse ($n = 6$). $^{**}P = 0.0022$; Mann–Whitney test, two-tailed. **b** Flow cytometry analysis of FOXP3⁺ Tregs in E21:I-A^{g7} and G20:I-A^{g7} tetramer-binding CD4⁺ T cells in SLOs of 6-week-old female NOD and NOD.Ins2^{-/-} mice. Data (mean ± s.e.m) summarize results from three independent experiments; each symbol represents results from an individual mouse ($n = 7$

for NOD E21 group, $n = 8$ for NOD.Ins2^{-/-} E21 group, $n = 6$ for NOD G20 group, $n = 7$ for NOD.Ins2^{-/-} group). ns, not significant; $^{****}P < 0.0001$; Mann–Whitney test, two-tailed. **c** ELISPOT assay for assessing T cell responses during antigen recall with intact insulin or Syn-E21 in NOD or NOD.Ins2^{-/-} mice post immunization with the B:9–23 peptide. Data (mean ± s.e.m) summarize results from three independent experiments; each symbol represents results from an individual mouse ($n = 5$). $^{**}P = 0.0079$; Mann–Whitney test, two-tailed. The schematic figure is created in BioRender. Wan, X. (2024) BioRender.com/h201924.

Discussion

The implications of β -cell crinophagy in T1D pathogenesis provide several new insights. First, we demonstrate that crinosomes, as a minor set of β -cell granules, adequately shape the MHC-II epitope repertoire in pancreatic islets. This finding aligns with our previous studies showing that peptides from crinosomes are highly compatible with MHC-II-bound epitopes identified in pancreatic islets and lymph

nodes³¹. Although crinosomes are much lower in number, the presentation of the crinosome-derived insulin G20 epitope in islets was at a similar level with the E21 epitope that mostly comes from DCGs. It is possible that epitopes like G20, which bypass epitope editing in APCs, are more efficiently presented by I-A^{g7} than the E21 epitope that is presented through the canonical intracellular pathway. Indeed, I-A^{g7} was shown to weakly interact with Class II-associated invariant chain

peptide (CLIP), and this rapid CLIP dissociation facilitated the presentation of extracellular peptides giving rise to G20⁷². This unconventional and less constrained presentation mode may also explain why epitopes from an unedited repertoire, which usually have lower MHC-II-binding affinities, can become a stable component of a self-peptidome. In general, the involvement of these unedited epitopes in autoimmunity may relate to the prominent role of low-affinity T cells in driving autoimmune responses^{73–75}.

Moreover, our data reinforce the role of crinophagy in generating post-translationally modified peptides recognized by autoreactive T cells^{31–33}. While the mechanisms involved in this process need further investigation, crinophagy may represent a mechanism through which physiologically generated PTMs can precipitate pathogenic outcomes in autoimmunity. These PTMs may trigger initial inflammatory and stress signals that are known to induce PTMs under pathological conditions^{76,77}, thus creating a feed-forward loop amplifying pathogenicity.

Although it has been increasingly recognized that β -cell functions may link to T1D pathogenesis, the identification of intrinsic β -cell targets for attenuating autoimmunity remains largely unexplored. We propose crinophagy as a potential therapeutic target, supported by evidence demonstrating that crinophagy inhibition reduced the generation of pathogenic insulin epitopes without affecting DCGs. The present study using chloroquine provides proof-of-concept evidence that diabetes inhibition could be achieved by impairing the formation of crinophagic granules. This mechanism extends the established view that chloroquine treats autoimmune diseases by directly inhibiting antigen processing in APCs. As a physiological process, peptides made in crinosomes can be available from the very beginning of autoimmune response development. Our results in NOD mice show that early intervention with chloroquine was able to delay diabetes progression and partially reduce disease incidence. This phenotype generally correlates to the observed effect of chloroquine in diminishing crinophagic granules and associated peptide production (by about 50%) in young NOD mice.

As diabetes develops, autoimmune responses are also driven by new epitopes resulting from inflammation and stress. The contribution of crinophagy in epitope spreading requires further investigation. We recently found substantially increased production of the immunogenic 6.9HIP in crinosomes from islets (young NOD mice) undergoing ER stress⁷⁸, suggesting that stress responses in β cells can be reflected in changes in epitope formation in crinosomes. A recent clinical trial tested the effect of hydroxychloroquine in autoantibody-positive (stage 1) T1D patients and found that hydroxychloroquine did not delay progression to stage 2 T1D but reduced autoantibody acquisition and titers of anti-insulin and anti-GAD antibodies⁷⁹. Since stage 1 T1D patients manifest multiple anti-islet autoantibodies, it is possible that hydroxychloroquine may not be sufficient for patients with potentially diversified pathogenic epitope repertoire. Young NOD mice showed similar insulin peptide levels in the crinosome fraction with B6g7 mice, suggesting that crinophagy functions normally at the onset of autoimmunity. However, crinophagy may be shaped by autoinflammatory and metabolic changes as diabetes advances. Although this area remains understudied, a previous study has noted a significant decrease in crinophagy (measured by proinsulin/lysosome colocalization) in diabetic T1D patients³⁶. Overall, our data suggest that crinophagy may need to be targeted before β cells become dysfunctional to obtain therapeutic benefits.

Nevertheless, a caveat in our experiments lies in potential off-target effects of chloroquine. Although our data suggest that the influence of chloroquine in islet presentation may outweigh its potential effect in thymic selection, the observed delay in diabetes development may result from chloroquine's effects in other tissue sites. Addressing this limitation requires further investigation of whether specific molecules expressed by crinosomes can be targeted for

precision therapy. The term crinophagy is often used interchangeably with (macro)autophagy; however, in β cells, crinophagy may function as a separate biological process from macroautophagy. Under starvation conditions, β cells, unlike many other mammalian cells, were shown to suppress macroautophagy, while activating lysosomal degradation of nascent insulin granules, a specific type of crinophagy⁸⁰. These findings suggest the possibility of specifically targeting crinophagy to avoid adverse effects associated with broadly disturbing autophagy. In fact, conditional deletion of key autophagy genes in β cells, including *Atg5*⁸¹ and *Atg7*⁸², resulted in profound phenotypes such as β -cell dysfunction, death, and hyperglycemia. Although crinophagy was described over 50 years ago, molecular mechanisms governing crinophagy, especially those that may uncouple crinophagy from macroautophagy, remain largely unknown. In this regard, recent studies aimed at dissecting molecules involved in delivering DCGs to lysosomes, such as Rab7 interacting lysosomal proteins (RILP)⁸³ and vesicle-associated membrane protein 4 (VAMP4)⁸⁴, represent a promising direction.

In this study, we sought to assess insulin epitopes that are naturally presented in the thymus without involving transgenic expression of synthetic antigens. This approach allowed us to detect the spontaneous, low-level presentation of the insulin E21 epitope by mTECs. We found that thymic insulin (E21) presentation efficiently mediated the differentiation of epitope-specific Tregs, consistent with studies indicating that PTA-specific CD4⁺ T cells are diverted into the Treg lineage^{85,86}. These results also bode well with strong evidence showing that the negative selection machinery in NOD mice is functional⁸⁷. Compared to their conventional T-cell phenotypes in the periphery, G20-specific T cells appear to acquire a Treg signature when migrating to pancreatic islets⁷². How this process influences the overall pathogenicity of these T cells and therapeutic applications requires further investigation. In addition to Treg conversion, a recent study has successfully identified high-affinity anti-insulin TCR clones in *Aire*-deficient mice, which are deleted in an *Aire*-dependent manner⁸⁸. However, central tolerance to insulin is limited at multiple levels. Reflecting a genetic difference, we did not detect the presentation of CP1 in the thymus. Given that CD4⁺ T cells recognizing native CP1 were mostly cross-reactive to the deamidated CP1d epitope³¹, this finding may explain the observed autoreactive phenotype in CP1d-specific T cells. In humans, polymorphisms upstream of the insulin gene promoter influence thymic insulin levels, with diabetes-protective alleles associated with higher thymic insulin levels^{89,90}. In mice, thymic insulin levels correlate with the copy number of the *Ins2* gene⁹¹. Such a role of gene expression is clearly reflected in our studies, showing that *Ins2* deficiency largely and selectively abolished E21-specific Treg differentiation.

By assessing the thymic MHC-II peptidome, we found that the majority of the thymic MHC-II epitopes originated from various peripheral tissues, many of which could be mapped to PTAs regulated by *Aire*, *Fezf2*, and *Chd4*. Considering sensitivity limitations in the immunopeptidome analysis, the actual scope of thymic PTA should be much broader than what has been revealed in the present study. This approach also allowed us to identify bona fide β -cell-derived epitopes that are naturally presented in the thymus, which are recognized by CD4 T cells exhibiting a Treg signature. Although these epitopes contribute to thymic selection, they may come from multiple sources not limited to the thymus. For example, ZnT8 expression has been shown to be low in human thymus⁹², suggesting that the identified thymic ZnT8 epitope comes from a peripheral source. This corresponds to studies showing that multiple mechanisms, such as thymic entry of blood-borne small proteins⁹³, acquisition of circulating proteins by thymic transendothelial DCs⁹⁴, and antigen transport by migratory APCs^{95,96}, contribute to diversifying the thymic epitope repertoire. Overall, it is evident that the thymic MHC-II peptidome is tightly linked and precisely shaped by the promiscuous PTA gene

expression program, a crucial concept thought to govern central tolerance but mostly established at the transcriptional level.

In summary, the present study indicates that the repertoire in pancreatic islets is diversified by the tissue-intrinsic mechanism, crinophagy, creating a peripheral–thymic mismatch underlying the activation of autoimmune T cells. It is conceivable that each peripheral tissue may use such mechanisms to generate a signature repertoire reflecting its anatomic features. This may also affect whether a tissue site would be susceptible to autoimmunity. Since its first discovery in the 1960s²⁴, crinophagy has been described in secretory cells in multiple endocrine tissues, including islets, thyroid, adrenal, and pituitary gland²⁷. Crinophagy may, therefore, be a common factor predisposing autoimmunity in these frequently targeted tissues.

Methods

Mice

NOD/ShiLtJ (NOD, stock #: 001976), NOD.129S2(B6)-*Ins2tm1Jja*/GseJ (NOD.*Ins2*^{−/−}, Stock #:005036), and NOD.Cg-Tg (*Ins2*^{*Y16A}) *1ElIns2tm1JjaIns2tm1Jja*/GseJ (NOD.B16A, Stock #:005524) were originally obtained from The Jackson Laboratory. NOD.10E11 TCR transgenic mice (TCRα: TRAV5D-4/TRAJ42; TCRβ: TRBV13-3/TRBD2/TRBJ2-7) were generated previously²⁸. All mice were bred, maintained, and used in experiments in our specific pathogen-free (SPF) animal facility in accordance with the guidelines of the Division of Comparative Medicine at Washington University School of Medicine (Association for Assessment and Accreditation of Laboratory Animal Care accreditation No. A3381-01; Protocol No. 23-0429).

Antibodies

For in vivo blockade treatment, rat IgG1 anti-mouse CD25 (PC61, Cat #: C2845), mouse IgG2b anti-CTLA4 (9D9, Cat #: C2856), and mouse IgG1 anti-TGF-β1,2,3 (1D11.16.8, Cat #: T799) were purchased from Leinco Technologies. For flow cytometry, we used the following fluorescently conjugated antibodies purchased from BioLegend: anti-CD45 (30-F11, Cat #: 103138), anti-CD11c (N418, Cat #: 117318), anti-CD11b (M1/70, Cat #: 101226), anti-CD3e (145-2C11, Cat #: 100306), anti-CD4 (RM4-5, Cat #: 100527), anti-CD8a (53-6.7, Cat #: 100732), anti-CD44 (IM7, Cat #: 103012), anti-CD28 (37.51, Cat #: 102106), anti-CD25 (PC61, Cat #: 102006), anti-EpCAM1 (G8.8, Cat #: 118214), anti-CD80 (16-10A1, Cat #: 104734), anti-CD90.2 (53-2.1, Cat #: 140306), anti-B220 (RA3-6B2, Cat #: 103234), anti-FR4 (12A5, Cat #: 125012), anti-CD69 (HL2F3, Cat #: 104512), and anti-TER-119 (TER-119, Cat #: 116203); or the following antibodies purchased from other companies: anti-CD45RA (14.8, BD Pharmingen, Cat #: 564359), anti-CD69 (HL2F3, Invitrogen, Cat #: 25-0691-82), anti-Ly51 (6C3, eBioscience, Cat #: 12-5891-82), anti-CD73 (TY/11.8, eBioscience, Cat #: 48-0731-82), anti-Foxp3 (FJK-16s, eBioscience, Cat #: 12-5773-82), and Rabbit anti-LAMP1 (EPR21026; Abcam, Cat #: ab208943). The anti-I-A^b antibody (AG2.42.7) and anti-insulin peptide antibodies (6F3 and AIP) were generated in our laboratory. Information related to antibodies can be found in Supplementary Data 5.

Transmission electron microscopy

For immunolocalization at the ultrastructural level, islets were fixed in 4% paraformaldehyde/0.05% glutaraldehyde (Polysciences, Cat #: 00380 and #07710) in 100 mM PIPES/0.5 mM MgCl₂, pH 7.2 for 1 hour at 4 °C. Samples were then embedded in 10% gelatin and infiltrated overnight with 2.3 M sucrose/20% polyvinyl pyrrolidone in PIPES/MgCl₂ at 4 °C. Samples were trimmed, frozen in liquid nitrogen, and sectioned with a Leica Ultracut UCT7 cryo-ultramicrotome (Leica Microsystems). Ultrathin sections of 50 nm were blocked with 5% FBS (Gibco, Cat #: 26140-087)/5% normal goat serum (ThermoFisher, Cat #: 50062Z) for 30 min and subsequently incubated with mouse anti-insulin B-chain (6F3) and rabbit anti-LAMP1 antibodies for 1 hour at room temperature. Following washes in block buffer, sections were

then incubated with goat anti-mouse IgG conjugated to 18 nm colloidal gold (Jackson ImmunoResearch Laboratories, Cat #: 115-215-146) and goat anti-rabbit IgG antibody conjugated to 12 nm colloidal gold (Jackson ImmunoResearch Laboratories, Cat #: 111-205-144) for 1 h. Sections were stained with 0.3% uranyl acetate/2% methyl cellulose and viewed on a JEOL 1200 EX transmission electron microscope (JEOL) equipped with an AMT 8-megapixel digital camera and AMT Image Capture Engine V602 software (Advanced Microscopy Techniques). All labeling experiments were conducted in parallel with controls omitting the primary antibody.

β-cell granule isolation and subsequent analysis

Islets were hand-picked and dispersed using a non-enzymatic dispersion solution (Sigma-Aldrich, Cat #: C5914) for 3 min at 37 °C. Islet cells were then washed and resuspended in 1.0 ml PBS. Cell lysis was accomplished by passing islet cells through a Cell Homogenizer (Isobiotec) 5 times using the 10 μm clearance ball bearing to shear the cells. Cell lysate was spun for 10 min at 1000g, 4 °C to pellet cell debris. The supernatant was transferred to a new tube, followed by a repeat of the 1000g spin. Pellets from both spins were discarded, and the supernatants were spun for 10 min at 5000g, 4 °C. The supernatant was transferred to a new tube, and the pellet was retained. Repeat the 5000g spin and transfer the supernatant to a clean tube. Pellets from both 5000g spins were combined into one tube (as the crinosome fraction) and suspended in media. The supernatant was spun for 20 min at 15,000g, and the pellet was retained. The supernatant was transferred to a new tube and was spun for 30 min at 25,000g, 4 °C. The pellet (as the DCG fraction) was suspended in media. For presentation, the fractions isolated by 5,000g (5k), 15,000 (15k), or 25,000g (25k) spins were offered to the C3.g7 APC line (B cell lymphoma expressing I-A^b; 5 × 10⁴/well) in a 96-well culture plate. After incubation for 2 h, the CD4⁺ T cell hybridomas (5 × 10⁴/well) were added. For mass spectrometry analysis, the subcellular fractions were frozen at −80 °C and thawed at 37 °C for five cycles to release the contents of granules. After freeze/thaw, a complete protease inhibitor cocktail was added to the sample, and they were concentrated by speed vac to a volume of ~100 μl. C18 Spin Columns (Pierce, Cat #: 89870) were used to clean up the released proteins/peptides according to the manufacturer's instructions. Samples were eluted in 0.1% formic acid (ThermoFisher, Cat #: A118-500)/95% acetonitrile (Burdick & Jackson, #015-4) and then dried with a Speed-Vac. Acid phosphatase activity in the granule contents was tested using an ELISA-based acid phosphatase assay kit (MilliporeSigma, Cat #: CS0740). Total protein levels in the granule contents were measured by a Micro BCA protein assay kit (Pierce, Cat #: 23225).

Treatment of mice with chloroquine

We primarily used two treatment regimens in this study. For most functional assays (peptidome, granule presentation, islet presentation), we used a “short-term” protocol, in which four doses of chloroquine MilliporeSigma, Cat #: C6628) in PBS were administered by intraperitoneal injections over a three-day period (two doses on the first day followed by one dose each on the next two days; 20 mg/kg per injection). The only variant of this short-term regimen was testing for blood leukocyte presentation, wherein mice received two chloroquine injections at 12 and 24 h before an in vivo glucose challenge. This adjustment was made in order to detect insulin peptides presentation by blood leukocytes, they need to be released into the circulation by glucose challenge. For monitoring diabetes development in NOD mice, female NOD mice were given chloroquine (20 mg/kg) in PBS via intraperitoneal injections twice a week starting from 21 days of age. The treatment was given for 3 weeks, paused for 1 week, and then resumed. Treatment was terminated when the mice became diabetic. These protocols are designed according to preliminary experiments suggesting that the effect of chloroquine in inhibiting G20

presentation lasts about three days. Diabetes development was monitored by checking urine and blood glucose levels weekly from 10 weeks of age. Diabetes is defined as blood glucose levels above 250 mg/dl for two consecutive measurements.

Histology and islet leukocyte infiltration score

Pancreata were fixed in 10% neutral buffered formalin (ThermoFisher, Cat #: SF93-4) and then embedded in paraffin, sectioned, and stained with hematoxylin and eosin. Microscopy imaging was performed using an EclipseE800 microscope (Nikon) equipped with CFI Plan Apo Lambda DM 20× air objective, X-Cite 120PC light source (Excelitas Technologies), EXi blue fluorescence microscopy camera, and QCapture 64-bit v2.9.13 acquisition software (QImaging). Islets were scored blindly. Islet scoring: 0, no insulinitis; 1, peri-insulinitis; 2, <25% of islet mass infiltrated; 3, 25–50% of islet mass infiltrated; 4, >50% of islet mass infiltrated.

Isolation of thymic APCs

Thymi were finely minced and gently stirred in DMEM media for 15 min to partially remove thymocytes. The supernatant was discarded, and the remaining tissues were digested using Liberase (100 µg/ml; Sigma-Aldrich, Cat #: 05401020001) and DNase I (20 µg/ml, Sigma-Aldrich, Cat #: 10104159001) in DMEM media at 37 °C for 30 min. The tissues were further disrupted by pipetting in ice-cold DMEM media to prepare single-cell suspensions. For the isolation of mTECs for antigen presentation, single-cell suspensions from WT NOD or B16A mice were subjected to CD45 microbeads, and the remaining cells were used for FACS sorting of mTECs. For the isolation of other thymic APCs for antigen presentation, Thy1.2 magnetic beads (Miltenyi Biotec, Cat #: 130-121-278) were used to remove the residual thymocytes, and the remaining cells were used for FACS sorting of the different subsets of APCs. For examination of the thymic peptidome, single-cell suspensions were prepared from WT NOD or NOD.*Rag1*^{−/−} mice. The cells were washed with 1× PBS, the supernatant was discarded, and the cell pellets were frozen at −80 °C. In one peptidome analysis, the single-cell suspension from WT NOD mice was further subjected to Thy1.2 magnetic beads to remove the remaining thymocytes. The remaining cells were then washed and frozen as pellets.

Isolation of pancreatic islets and islet APCs

To isolate pancreatic islets and islet APCs, the peritoneal cavity was dissected to expose the common bile duct. Under a dissection microscope, the bile duct leading into the duodenum was clamped. Through the common bile duct, 5 mL of type XI collagenase (0.4 mg/mL in serum-free DMEM; Sigma-Aldrich, Cat #: C7657) digestion buffer was injected to inflate the pancreas. The inflated pancreas was carefully removed and placed in a 2-oz wide-mouth glass jar containing 5 mL of digestion buffer. It was then digested at a 37 °C water bath for 12 min without shaking. Afterwards, the jars were taken out and shaken vigorously for 90 s. The pancreata were washed three times with serum-free DMEM through a stainless tea strainer. The flowthroughs, which contained islets, were passed through a 70-µm cell strainer to retain the islets. The islets retained on the cell strainer were flushed from the filter onto a Petri dish for hand-picking. Pure hand-picked islets were dispersed using Cell Dissociation Solution Non-Enzymatic (Sigma-Aldrich, Cat #: C5914) for 10 min at 37 °C. To further isolate islet APCs, single-cell suspensions were washed and treated with Fc block antibody (clone 2.4G2) conditioned FACS buffer at 4 °C for 15 min. Cells were then stained with fluorescent antibodies for FACS sorting to isolate islet macrophages, cDC1, and cDC2.

Antigen presentation assay

Epitope-specific CD4⁺ T cell hybridomas were cultured with different source APCs in round-bottom 96-well plates in the absence of

exogenous antigen stimulation to test spontaneous presentation. In some experiments, exogenous antigens were used for stimulation. Each well contained 50,000 CD4⁺ T cell hybridomas and the respective APCs: mTECs (150,000), other thymic APCs (cDC1, cDC2, B cells, pDCs; 50,000 for each), dispersed islet cells (50,000), islet APCs (cDC1, cDC2, resident macrophages; 1,000 for each), or C3.g7 (50,000). After an overnight incubation, T-cell responses were assessed by measuring IL-2 production in the culture supernatants. In most experiments, IL-2 production was measured using the IL-2-dependent cell line, CTLL-2, and the proliferation of CTLL-2 cells was determined by the incorporation of ³H thymidine (cpm). In some experiments, IL-2 production was quantified in the culture supernatants using ELISA (units/ml). Both assays show similar sensitivity and detection ranges.

Isolation of the thymic MHC-II peptidome

Thymic cells were collected from 155 NOD mice (−150 × 10⁹ cells after thymocyte removal by gentle agitation), 71 unmanipulated NOD.*Rag1*^{−/−} mice (−3 × 10⁹ cells), or 71 NOD mice with further thymocyte removal by magnetic beads (−3 × 10⁹ cells). For each of the three independent analyses, the frozen cell pellets were thawed on the isolation day and suspended in fresh lysis buffer (40 mM MEGA 8 (MilliporeSigma, Cat #: O3129), 40 mM MEGA 9 (MilliporeSigma, Cat #: N1138), 1 mM phenylmethylsulfonyl fluoride (MilliporeSigma, Cat #: P7626), 0.2 mM iodoacetamide (MilliporeSigma, Cat #: I6125), 20 µg/ml leupeptin (MilliporeSigma, Cat #: L2884), and Roche complete Mini Protease cocktail (Roche Diagnostics, Cat #: 11836153001) in PBS). The suspension was rocked for 2 h at 4 °C. The cell lysate was then centrifuged at 20,000×g for 30 min at 4 °C. To eliminate non-specific binding of peptides, the supernatant was first incubated with polyclonal mouse IgG (Leinco, Cat #: N229; 1.5 mg antibody per sample) bound to Sepharose 4B (MilliporeSigma, Cat #: C9142) at 4 °C for 30 min. The unbound material containing peptide-MHC-II complexes was collected and added to a tube containing PBS-washed sepharose conjugated to the anti-I-A^b antibody (AG2.42.7; 3.0 mg per sample). This mixture was incubated at 4 °C overnight. The I-A^b-sepharose was applied to a column and washed four times as follows: 10 ml 150 mM NaCl and 20 mM Tris (pH 7.4), 10 ml 400 mM NaCl and 20 mM Tris (pH 7.4), 10 ml 150 mM NaCl and 20 mM Tris (pH 7.4), and 10 ml 20 mM Tris (pH 8.0). Peptides were eluted with 10% acetic acid (ThermoFisher, Cat #: A38SI-212) and dried using a SpeedVac. Eluted peptides were resuspended and passed over detergent removal spin columns (Pierce, Cat #: 87777) to remove traces of remaining detergent, and then cleaned using C18 Spin Columns (Pierce, Cat #: 89870). For enriching insulin B-chain peptides by antibody capture, the sample after the 10% acetic acid elution was dried down. Upon resuspension in PBS, the sample was incubated overnight at 4 °C with sepharose conjugated to two monoclonal antibodies (0.5 mg per sample): AIP and 6F3. The antibody-sepharose was applied to a column and washed as described above. Peptides captured by the antibody mixture were eluted with 10% acetic acid and dried prior to detergent removal and cleaning using spin columns.

Mass spectrometry

A Dionex UltiMate 3000 system (Thermo Scientific) was coupled to an Orbitrap Fusion Lumos mass spectrometer (Thermo Scientific) through an Easy-Spray ion source (Thermo Scientific). Each crinosome peptidome (PBS and chloroquine) and thymic MHC-II peptidome (NOD mice, NOD.*Rag1*^{−/−} mice, NOD mice with T cell depletion) corresponded to an independent biological sample analyzed by mass spectrometry. Peptide samples were dissolved in 2% acetonitrile/0.1% formic acid (20 µL) and loaded as a single injection (19 µL, 15 µL/min, 3 min) onto a trap column (100 µm × 2 cm, 50 °C, 5 µm Acclaim PepMap 100 C18, Cat #: 164946). The peptides were then eluted at a flow rate of 0.200 µL/min onto an Easy-Spray PepMap RSLC C18 column (2 µm,

50 cm × 75 μm ID, 50 °C, Thermo Scientific, Cat #: ES803) and separated using the following gradient, all in terms of % Buffer B (0.1% formic acid in ACN, Honeywell, Fisher Scientific, Cat #: 6000053; Buffer A: 0.1% formic acid in the water, Honeywell, Fisher Scientific, Cat #: 6003079): 0–110 min, 2–22%; 110–120 min, 22–35%; 120–130 min, 35–95%; 130–150 min, isocratic at 95%; 151–153 min, 95–2%; 153–171 min, isocratic at 2%. The spray voltage was set to 1700 V, the ion transfer tube temperature was set to 275 °C, and the RF lens was set to 30%. MS scans were acquired in profile mode and MS/MS scans in centroid mode for ions with charge states 2–5, with a cycle time of 3 s. MS spectra were recorded from 375 to 1500 Da at a resolution of 120 K (at *m/z* 200), and HCD MS/MS was triggered above a threshold of 2.0e4. Quadrupole isolation was set at 0.7 Da with a resolution of 30 K, and collision energy (CE) was set to 30%. Dynamic exclusion was implemented with a window of ±5 ppm for 60 s, and monoisotopic precursor selection was used.

Mass spectrometry data analysis

The data files were processed, de novo sequenced, and searched against the UniProt Mouse database (downloaded 5/4/2021; 22,105 entries) appended with the Common Repository for Adventitious Proteins (cRAP) contaminant database using PEAKS X+ software (Bioinformatics Solutions). Mass error tolerances of 10 ppm and 0.01 Da were set for parent and fragment ions, respectively. Enzyme specificity was not specified, and variable modifications included methionine oxidation, deamidation of glutamine and asparagine, carbamidomethylation of cysteine, and oxidation of cysteine to cysteic acid. False discovery rate (FDR) estimation was enabled, and filters were adjusted to achieve a 1% FDR at the peptide level. To identify HIPs, multi-round searching was performed using the mouse portion of an *in silico* HIP database⁵⁰. Peptides passing the 1% FDR filter were exported, and HIPs were further validated as described previously⁵¹. Briefly, MS/MS spectra assigned to HIPs were filtered to ensure that they could not be assigned to modified forms of abundant canonical peptides by comparison to the SPIDER search results. The remaining spectra were manually verified to ensure the presence of sufficient fragment ions to support the assignment. Spectra that passed these filters were further validated by comparison to synthetic standards.

Further analysis of the thymic MHC-II peptidome data

To identify tissues and organs in which parent proteins of the thymic MHC-II peptides were expressed, and their corresponding cell components and cellular location, the Uniprot identifiers were uploaded to the Database for Annotation, Visualization, and Integrated Discovery (DAVID), and a functional annotation chart was generated. To identify the corresponding transcriptional regulators for tissue-specific antigens identified in the thymic peptidome, the complete dataset from Tomofuji et al. (ref. 63) was downloaded and filtered to obtain significantly regulated genes for Aire, Fezf2, and Chd4 in mTECs from C57BL/6 mice. These lists were then used to identify protein products of regulated genes in the thymic peptidome by querying the complete list of parent proteins against the lists of significantly regulated genes. A similar approach was used to overlay the peptidome data with single-cell RNA sequencing analysis from Michelson et al (ref. 65) to identify PTA also expressed by mimetic mTEC subtypes. The differentially expressed genes were defined by the same criteria used in the original studies.

Competition binding assay

To evaluate relative MHC-II-binding affinities of identified peptides (competitors), C3.g7 cells (10⁴) were mixed with competitor peptides and incubated for 30 min at 37 °C. The HEL:II–25 peptide (1 μM) was added to the C3.g7/competitor peptide mixture and incubated for an additional 60 min at 37 °C. Cells were spun down and washed. A CD4⁺ T cell hybridoma specific for the HEL:II–25 peptide (clone 10E11) was

added to the washed and loaded C3.g7 cells and incubated overnight at 37 °C. The supernatants were then collected, and the production of IL-2 was measured by ELISA. IC50 values for competitor peptides were generated by fitting the data using GraphPad Prism software as a four-parameter inhibitor vs response curve.

Tetramer staining using magnetic enrichment

The generation of I-A^{b7}-based monomers has been described previously⁵. The biotinylated monomers were tetramerized at room temperature for 1 h using APC or PE-labeled Streptavidin (Agilent Technologies, Cat #: PJ27S and PJRS301-1) at a 5:1 molar ratio of biotinylated molecules to labeled streptavidin. Single cells prepared from the spleen and lymph nodes were washed with phosphate-buffered saline (PBS) twice and incubated with APC or PE-labeled tetramers at a final concentration of 10 μg/ml for 1 h at room temperature. The cells were washed with MACS buffer (2 mM EDTA, 0.5% BSA in PBS) twice and then incubated with 20 μl anti-APC or PE microbeads (Miltenyi Biotec, Cat #: 130-090-855 and 130-048-801) in 100 μl MACS buffer at 4 °C for 20 min. The mixture was washed and resuspended in 1 ml MACS buffer and applied to LS columns (Miltenyi Biotec, Cat #: 130-042-401). Both the flow-through (negative) and the column-bound cells (positive) were collected for flow cytometry analysis. The tetramer-positive cells were mostly in the positive portion. The negative portion was collected to evaluate the efficiency of the selection and for quantification.

Flow cytometry and cell sorting

Spleens and lymph nodes were collected and meshed through a 70 μm cell strainer, and red blood cells were lysed by red blood cell lysis buffer (ACK buffer) to make single-cell suspensions. Thymi were collected with fat tissues removed and digested with 100 μg/ml of Liberase and 20 μg/ml of DNase I in DMEM solution at 37 °C for 30 min to prepare a single-cell suspension. The separated cell portions after tetramer incubation were collected for staining. To block Fc-receptors engaging, the cell suspensions were incubated at 4 °C for 5 min in PBS (pH 7.4) supplemented with 2% FBS (fetal bovine serum) and 50% of Fc-block (made in-house). For surface staining, cells were incubated with fluorescently labeled antibodies (1:200 [vol/vol]) at 4 °C for 20 min. Cells were then washed and analyzed by flow cytometry or subjected to FACS sorting. For staining of intracellular transcription factors, islet cells were stained with surface antibodies for 20 min, fixed, and permeabilized using the FOXP3 transcription factor staining buffer set (Thermo Fisher Scientific, Cat #: 00-5523-00) per the manufacturer's instructions. Cells were incubated with the anti-FOXP3 antibody at room temperature for 30 min. To sort the antigen-specific T cells for scRNA-seq analysis, two sets of tetramers were individually conjugated with APC-labeled Streptavidin at a 5:1 molar ratio at room temperature for at least 1 h. The thymic epitope set included CP2, E21, DBP, ZnT8, and the islet set included CP1d, G20, 2.SHIP, 6.9HIP epitopes. After conjugation, four individual tetramers in the thymic or islet epitope set were combined. For the first experiment, 14 mice were used for thymic epitope-specific T cells, and 6 mice were used for islet epitope-specific T cells. In the second experiment, 10 mice were used for thymic epitope-specific T cells, and 4 mice were used for islet epitope-specific T cells. SLOs from two mice were combined as one sample for isolation. After red blood cell lysis, cells were washed with MACS buffer, and the CD19⁺ B cells and CD11b⁺ myeloid cells were depleted by CD19 beads (Miltenyi Biotec, Cat #: 130-050-301, 120 μl for each sample) and CD11b beads (Miltenyi Biotec, Cat #: 130-097-142, 80 μl for each sample). After depletion, the cells were washed twice with PBS and incubated with the two sets of combined tetramers at room temperature for 1 h with shaking. After incubation, cells were washed with MACS buffer and incubated with 40 μl of anti-APC microbeads at 4 °C for 20 min. Tetramer-positive cells were enriched using LS columns. 10E11 CD4⁺ T cells were prepared by meshing the spleen through

a 70 µm strainer, lysing the red blood cells, and enriched using the naïve CD4⁺ T Cell Isolation Kit (Miltenyi Biotec). Before surface staining, samples were incubated with 100 µl of TotalSeq™ anti-mouse Hashtag reagent (1:100 [vol/vol], BioLegend) to tag the samples: enriched cells from the islet epitope set were tagged with the TotalSeq-C0301 anti-mouse Hashtag 1 Antibody (Barcode sequence: ACCCACAGTAAGAC); enriched cells from the thymic epitope set were tagged with the TotalSeq-C0302 anti-mouse Hashtag 2 Antibody (Barcode sequence: GGTGAGAGCATTCAT); 10E11 naïve CD4⁺ T cells were tagged with the TotalSeq-C0303 anti-mouse Hashtag 3 Antibody (Barcode sequence: CTTGCCGATGTCAT). Then, 2× antibody mixtures (1:100 [vol/vol]) for surface staining were prepared. For cells with tetramer staining, PE-anti-Thy1.2, eFluor450-anti-CD73, PE-Cy7-anti-CD4, PercP-eFluor710-anti-CD8, eFluor780-Fixable Viability Dye, AF488-anti-B220, I-A^{b7}, and CD11b were used. For 10E11 naïve T cells, APC-anti-CD62L, PE-anti-Thy1.2, BV421-anti-CD44, PE-Cy7-anti-CD4, PercP-anti-CD25, CD69, eFluor 780-Fixable Viability Dye, AF488-anti-B220, I-A^{b7}, and CD11b were used. After incubating for 20 min at 4 °C, cells were washed twice with FACS buffer. Regular flow cytometry samples were analyzed by BD FACSCanto II (BD Biosciences), and FACS cell sorting was performed using the BD FACSARIA II sorter (BD Biosciences). All the data were analyzed using the FlowJo 10.0 software (Tree Star).

Quantification of tetramer-binding T cells

The quantification of tetramer-binding T cells was performed according to the previously described methodology⁶⁹. Briefly, cell-counting beads (Invitrogen, Cat #: PCB100) were diluted to a concentration of 200,000 beads/ml with MACS buffer. A 200 µl aliquot of the bead solution was mixed with 5 µl of cells from both portions (positive and negative) after selection. The final volume of the positive portion was 200 µl, while the final volume of the negative portion was 2 ml. To calculate the total cell number, the following equation was used: Total cell number = (cell events/bead events) × (bead concentration) × (bead volume/cell volume) × (volume of cell sample).

Antigen-specific T cell responses by ELISPOT assay

For evaluating T cell responses by immunization, mice were immunized with the indicated peptides (25 nmol) emulsified with CFA at the footpad. On day 7, the popliteal lymph node cells were restimulated with the indicated peptides (10 µM) for 24 hours, and IFN γ production was assessed by ELISPOT. In some experiments, mice were injected intraperitoneally with anti-CD25 (2 mg), anti-CTLA4 (250 µg), or anti-TGF β (2 mg) on day 1, followed by additional injections of each antibody (250 µg) on day 3 and 6, before harvesting the popliteal lymph node cells. To evaluate T cell responses in islets and pancreatic lymph nodes without immunization, total islet, and pancreatic lymph node cells were mixed and cultured in DMEM containing 10% FBS at a concentration of 2 × 10⁶ cells/ml media. The culture was supplemented with 20 U/ml IL-2 and 1 µM peptides to stimulate T cell replication and incubated at 37 °C for 7 days. Total live cells were collected from the culture using Histopaque 1119 and subjected to a second round of amplification. The live cells were added to a culture containing 20 U/ml IL-2 and 1 µM peptide as before, along with 2 × 10⁶ irradiated NOD splenocytes (3000 RAD) per ml of culture. This culture was incubated for 3 days at 37 °C. In all experiments, cells were harvested and assayed for reactivity by eliciting a recall response on IFN γ -coated 96-well multi-screen plates (BD Biosciences, Cat #: 551881) for ELISPOT. The reactive cells were counted using Immunospot Software (C.T.L.).

Library preparation for single-cell RNA sequencing analysis

cDNA was prepared after the GEM generation and barcoding, followed by the GEM-RT reaction and bead cleanup steps. Purified cDNA was amplified for 11–16 cycles before being cleaned up using SPRIselect beads. Samples were then run on a Bioanalyzer to determine the cDNA concentration. V(D)J target enrichment (TCR) was performed on the

full-length cDNA. Gene Expression, Enriched TCR, and Feature libraries were prepared according to the recommended protocols from the 10× Genomics Chromium Single Cell 5' Reagent Kits User Guide (v2 Chemistry Dual Index) with Feature Barcoding technology for Cell Surface Protein and Immune Receptor Mapping, with appropriate modifications to the PCR cycles based on the calculated cDNA concentration. For sample preparation on the 10× Genomics platform, the following kits were used: Chromium Next GEM Single Cell 5' Kit v2, 16 rxns (Cat #: PN-1000263), Chromium Next GEM Chip K Single Cell Kit, 48 rxns (Cat #: PN-1000286), Chromium Single Cell Human TCR Amplification Kit (Cat #: PN-1000252), Dual Index Kit TT Set A, 96 rxns (Cat #: PN-1000215), 5' Feature Barcode Kit, 16 rxns (Cat #: PN-1000256), and Dual Index Kit TN Set A, 96 rxns (Cat #: PN-1000250). The concentration of each library was accurately determined through qPCR using the KAPA library Quantification Kit according to the manufacturer's protocol (KAPA Biosystems/Roche) to achieve the desired cluster counts for the Illumina NovaSeq6000 instrument. Normalized libraries were sequenced on a NovaSeq6000 S4 Flow Cell using the XP workflow and a 151 × 10 × 10 × 151 sequencing recipe according to the manufacturer's protocol. A median sequencing depth of 50,000 reads/cell was targeted for each Gene Expression library, and 5000 reads/cell for each V(D)J and Feature library.

Single-cell RNA sequencing data analysis

Libraries were counted using Cell Ranger (v7.1.0). Low-quality barcodes and UMIs were filtered and mapped to the mouse genome (mm10). Both datasets were further aggregated using the Cell Ranger aggr pipeline (v7.1.0). The Cell Ranger aggr pipeline automatically equalize the average read depth between samples. The gene expression from both data was filtered, normalized, and clustered, and the resulting Cloupe file was created and imported into the Loupe Browser for further analyses and visualization. To further define the unique molecular feature of the cell population in the study, the feature barcode approach was employed to quantify each feature in each cell. The expression levels of cell surface proteins were measured via an antibody and antigen-multimer staining assay using TotalSeq-C. The Cell Ranger (v7.1.0) pipeline outputs the feature barcode counts for each cell barcode. Specific antibody detection and filtering were performed as follows: the log2 count of target ≥ 10 , while the other log2 counts ≤ 6 . PCA was performed to reduce the dimensionality of the dataset to its most important features, and the principal components were visualized by tSNE or UMAP plots. The final analysis excluded cells with any expression of *Cd19*, *Lyz2*, and *H2-Ab1* transcripts. The differentially expressed genes between clusters or libraries were identified using default algorithms. Bonferroni-adjusted *p*-values were used to determine significance at an FDR < 0.05.

Reporting summary

Further information on research design is available in the Nature Portfolio Reporting Summary linked to this article.

Data availability

Mass spectrometry data are available via ProteomeXchange with the identifier [PXD030999](https://www.ebi.ac.uk/psd/entry/PXD030999). Single-cell RNA sequencing (GEO: GSE275211) [<https://www.ncbi.nlm.nih.gov/geo/query/acc.cgi?acc=GSE275211>] data were deposited in the National Center for Biotechnology Information Gene Expression Omnibus database. All the data generated in this study are provided in the Supplementary Tables/Source Data file. Source data are provided in this paper.

References

1. Todd, J. A., Bell, J. I. & McDevitt, H. O. HLA-DQ beta gene contributes to susceptibility and resistance to insulin-dependent diabetes mellitus. *Nature* **329**, 599–604 (1987).

2. Acha-Orbea, H. & McDevitt, H. O. The first external domain of the nonobese diabetic mouse class II I-A beta chain is unique. *Proc. Natl Acad. Sci. USA* **84**, 2435–2439 (1987).
3. James, E. A., Mallone, R., Kent, S. C. & DiLorenzo, T. P. T-cell epitopes and neo-epitopes in type 1 diabetes: a comprehensive update and reappraisal. *Diabetes* **69**, 1311–1335 (2020).
4. Roep, B. O., Thomaidou, S., van Tienhoven, R. & Zaldumbide, A. Type 1 diabetes mellitus as a disease of the β -cell (do not blame the immune system?). *Nat. Rev. Endocrinol.* **17**, 150–161 (2021).
5. Gioia, L. et al. Position β 57 of I-Ag7 controls early anti-insulin responses in NOD mice, linking an MHC susceptibility allele to type 1 diabetes onset. *Sci. Immunol.* **4**, eaaw6329 (2019).
6. Corper, A. L. et al. A structural framework for deciphering the link between I-Ag7 and autoimmune diabetes. *Science* **288**, 505–511 (2000).
7. Latek, R. R. et al. Structural basis of peptide binding and presentation by the type I diabetes-associated MHC class II molecule of NOD mice. *Immunity* **12**, 699–710 (2000).
8. Lee, K. H., Wucherpfennig, K. W. & Wiley, D. C. Structure of a human insulin peptide-HLA-DQ8 complex and susceptibility to type 1 diabetes. *Nat. Immunol.* **2**, 501–507 (2001).
9. Zhang, L., Nakayama, M. & Eisenbarth, G. S. Insulin as an autoantigen in NOD/human diabetes. *Curr. Opin. Immunol.* **20**, 111–118 (2008).
10. Unanue, E. R. Antigen presentation in the autoimmune diabetes of the NOD mouse. *Annu. Rev. Immunol.* **32**, 579–608 (2014).
11. Yu, L. et al. Early expression of antiinsulin autoantibodies of humans and the NOD mouse: evidence for early determination of subsequent diabetes. *Proc. Natl Acad. Sci. USA* **97**, 1701–1706 (2000).
12. Kendall, P. L. et al. Tolerant anti-insulin B cells are effective APCs. *J. Immunol.* **190**, 2519–2526 (2013).
13. Wan, X., Thomas, J. W. & Unanue, E. R. Class-switched anti-insulin antibodies originate from unconventional antigen presentation in multiple lymphoid sites. *J. Exp. Med.* **213**, 967–978 (2016).
14. Sharma, S. et al. Measuring anti-islet autoimmunity in mouse and human by profiling peripheral blood antigen-specific CD4 T cells. *Sci. Transl. Med.* **15**, eade3614 (2023).
15. French, M. B. et al. Transgenic expression of mouse proinsulin II prevents diabetes in nonobese diabetic mice. *Diabetes* **46**, 34–39 (1997).
16. Jaeckel, E., Lipes, M. A. & von Boehmer, H. Recessive tolerance to preproinsulin 2 reduces but does not abolish type 1 diabetes. *Nat. Immunol.* **5**, 1028–1035 (2004).
17. Thébault-Baumont, K. et al. Acceleration of type 1 diabetes mellitus in proinsulin 2-deficient NOD mice. *J. Clin. Invest.* **111**, 851–857 (2003).
18. Moriyama, H. et al. Evidence for a primary islet autoantigen (preproinsulin 1) for insulinitis and diabetes in the nonobese diabetic mouse. *Proc. Natl Acad. Sci. USA* **100**, 10376–10381 (2003).
19. Elso, C. M. et al. Replacing murine insulin 1 with human insulin protects NOD mice from diabetes. *PLoS ONE* **14**, e0225021 (2019).
20. Skovsø, S. et al. β -cell Cre expression and reduced *Ins1* gene dosage protect mice from type 1 diabetes. *Endocrinology* **163**, bqac144 (2022).
21. Jhala, G. et al. Tolerance to proinsulin-1 reduces autoimmune diabetes in NOD mice. *Front. Immunol.* **12**, 645817 (2021).
22. Nakayama, M. et al. Prime role for an insulin epitope in the development of type 1 diabetes in NOD mice. *Nature* **435**, 220–223 (2005).
23. Derbinski, J., Schulte, A., Kyewski, B. & Klein, L. Promiscuous gene expression in medullary thymic epithelial cells mirrors the peripheral self. *Nat. Immunol.* **2**, 1032–1039 (2001).
24. Smith, R. E. & Farquhar, M. G. Lysosome function in the regulation of the secretory process in cells of the anterior pituitary gland. *J. Cell Biol.* **31**, 319–347 (1966).
25. Halban, P. A. & Wollheim, C. B. Intracellular degradation of insulin stores by rat pancreatic islets in vitro. An alternative pathway for homeostasis of pancreatic insulin content. *J. Biol. Chem.* **255**, 6003–6006 (1980).
26. Orci, L. et al. Insulin, not C-peptide (proinsulin), is present in cisternophagic bodies of the pancreatic B-cell. *J. Cell Biol.* **98**, 222–228 (1984).
27. Weckman, A. et al. Autophagy in the endocrine glands. *J. Mol. Endocrinol.* **52**, R151–R163 (2014).
28. Wan, X. et al. Pancreatic islets communicate with lymphoid tissues via exocytosis of insulin peptides. *Nature* **560**, 107–111 (2018).
29. Mohan, J. F. et al. Unique autoreactive T cells recognize insulin peptides generated within the islets of Langerhans in autoimmune diabetes. *Nat. Immunol.* **11**, 350–354 (2010).
30. Mohan, J. F., Petzold, S. J. & Unanue, E. R. Register shifting of an insulin peptide-MHC complex allows diabetogenic T cells to escape thymic deletion. *J. Exp. Med.* **208**, 2375–2383 (2011).
31. Wan, X. et al. The MHC-II peptidome of pancreatic islets identifies key features of autoimmune peptides. *Nat. Immunol.* **21**, 455–463 (2020).
32. Reed, B. et al. Lysosomal cathepsin creates chimeric epitopes for diabetogenic CD4 T cells via transpeptidation. *J. Exp. Med.* **218**, e20192135 (2021).
33. Crawford, S. A. et al. Cathepsin D drives the formation of hybrid insulin peptides relevant to the pathogenesis of type 1 diabetes. *Diabetes* <https://doi.org/10.2337/db22-0303> (2022).
34. Zakharov, P. N., Hu, H., Wan, X. & Unanue, E. R. Single-cell RNA sequencing of murine islets shows high cellular complexity at all stages of autoimmune diabetes. *J. Exp. Med.* **217**, e20192362 (2020).
35. Mauthe, M. et al. Chloroquine inhibits autophagic flux by decreasing autophagosome-lysosome fusion. *Autophagy* **14**, 1435–1455 (2018).
36. Muralidharan, C. et al. Pancreatic beta cell autophagy is impaired in type 1 diabetes. *Diabetologia* **64**, 865–877 (2021).
37. Vomund, A. N. et al. Beta cells transfer vesicles containing insulin to phagocytes for presentation to T cells. *Proc. Natl Acad. Sci. USA* **112**, E5496–E5502 (2015).
38. Srivastava, N. et al. Chromogranin A deficiency confers protection from autoimmune diabetes via multiple mechanisms. *Diabetes* **70**, 2860–2870 (2021).
39. Calderon, B. et al. The pancreas anatomy conditions the origin and properties of resident macrophages. *J. Exp. Med.* **212**, 1497–1512 (2015).
40. Ferris, S. T. et al. The islet-resident macrophage is in an inflammatory state and senses microbial products in blood. *J. Exp. Med.* **214**, 2369–2385 (2017).
41. Zinselmeyer, B. H. et al. The resident macrophages in murine pancreatic islets are constantly probing their local environment, capturing beta cell granules and blood particles. *Diabetologia* **61**, 1374–1383 (2018).
42. Carrero, J. A. et al. Resident macrophages of pancreatic islets have a seminal role in the initiation of autoimmune diabetes of NOD mice. *Proc. Natl Acad. Sci. USA* **114**, E10418–E10427 (2017).
43. Srivastava, N. et al. CXCL16-dependent scavenging of oxidized lipids by islet macrophages promotes differentiation of pathogenic CD8⁺ T cells in diabetic autoimmunity. *Immunity* **57**, 1629–1647.e8 (2024).
44. Levisetti, M. G., Suri, A., Frederick, K. & Unanue, E. R. Absence of lymph nodes in NOD mice treated with lymphotoxin-beta receptor immunoglobulin protects from diabetes. *Diabetes* **53**, 3115–3119 (2004).
45. Gagnerault, M.-C., Luan, J. J., Lotton, C. & Lepault, F. Pancreatic lymph nodes are required for priming of beta cell reactive T cells in NOD mice. *J. Exp. Med.* **196**, 369–377 (2002).

46. Vomund, A. N. et al. Blood leukocytes recapitulate diabetogenic peptide-MHC-II complexes displayed in the pancreatic islets. *J. Exp. Med.* **218**, e20202530 (2021).
47. Delong, T. et al. Pathogenic CD4 T cells in type 1 diabetes recognize epitopes formed by peptide fusion. *Science* **351**, 711–714 (2016).
48. Wiles, T. A. et al. An insulin-IAPP hybrid peptide is an endogenous antigen for CD4 T cells in the non-obese diabetic mouse. *J. Autoimmun.* **78**, 11–18 (2017).
49. Baker, R. L. et al. CD4 T cells reactive to hybrid insulin peptides are indicators of disease activity in the NOD mouse. *Diabetes* **67**, 1836–1846 (2018).
50. Wiles, T. A. et al. Identification of hybrid insulin peptides (HIPs) in mouse and human islets by mass spectrometry. *J. Proteome Res.* **18**, 814–825 (2019).
51. Lichti, C. F. Identification of spliced peptides in pancreatic islets uncovers errors leading to false assignments. *Proteomics* **21**, 2000176 (2021).
52. Bräunlein, E. & Krackhardt, A. M. Identification and characterization of neoantigens as well as respective immune responses in cancer patients. *Front. Immunol.* **8**, 1702 (2017).
53. Yarchoan, M., Johnson, B. A., Lutz, E. R., Laheru, D. A. & Jaffee, E. M. Targeting neoantigens to augment antitumour immunity. *Nat. Rev. Cancer* **17**, 209–222 (2017).
54. So, M. et al. Proinsulin C-peptide is an autoantigen in people with type 1 diabetes. *Proc. Natl Acad. Sci. USA* **115**, 10732–10737 (2018).
55. Clement, C. C. et al. Autoimmune response to transthyretin in juvenile idiopathic arthritis. *JCI Insight* **1**, e85633 (2016).
56. Latorre, D. et al. T cells in patients with narcolepsy target self-antigens of hypocretin neurons. *Nature* **562**, 63–68 (2018).
57. Klein, L., Kyewski, B., Allen, P. M. & Hogquist, K. A. Positive and negative selection of the T cell repertoire: what thymocytes see (and don't see). *Nat. Rev. Immunol.* **14**, 377–391 (2014).
58. Suri, A., Walters, J. J., Gross, M. L. & Unanue, E. R. Natural peptides selected by diabetogenic DQ8 and murine I-A(g7) molecules show common sequence specificity. *J. Clin. Invest.* **115**, 2268–2276 (2005).
59. Huang, D. W., Sherman, B. T. & Lempicki, R. A. Systematic and integrative analysis of large gene lists using DAVID bioinformatics resources. *Nat. Protoc.* **4**, 44–57 (2009).
60. Anderson, M. S. et al. Projection of an immunological self shadow within the thymus by the aire protein. *Science* **298**, 1395–1401 (2002).
61. Meredith, M., Zemmour, D., Mathis, D. & Benoist, C. Aire controls gene expression in the thymic epithelium with ordered stochasticity. *Nat. Immunol.* **16**, 942–949 (2015).
62. Takaba, H. et al. Fezf2 orchestrates a thymic program of self-antigen expression for immune tolerance. *Cell* **163**, 975–987 (2015).
63. Tomofuji, Y. et al. Chd4 choreographs self-antigen expression for central immune tolerance. *Nat. Immunol.* **21**, 892–901 (2020).
64. Skogberg, G., Teleme, E. & Ekwall, O. Exosomes in the thymus: antigen transfer and vesicles. *Front. Immunol.* **6**, 366 (2015).
65. Michelson, D. A., Hase, K., Kaisho, T., Benoist, C. & Mathis, D. Thymic epithelial cells co-opt lineage-defining transcription factors to eliminate autoreactive T cells. *Cell* **185**, 2542–2558.e18 (2022).
66. Dai, J. et al. Enrichment and identification of cysteine-containing peptides from tryptic digests of performic oxidized proteins by strong cation exchange LC and MALDI-TOF/TOF MS. *Anal. Chem.* **77**, 7594–7604 (2005).
67. Collado, J., Guitart, C., Ciudad, M. T., Alvarez, I. & Jaraquemada, D. The repertoires of peptides presented by MHC-II in the thymus and in peripheral tissue: a clue for autoimmunity? *Front. Immunol.* **4**, 442 (2013).
68. Raposo, B. et al. T cells specific for post-translational modifications escape intrathymic tolerance induction. *Nat. Commun.* **9**, 353 (2018).
69. Moon, J. J. et al. Tracking epitope-specific T cells. *Nat. Protoc.* **4**, 565–581 (2009).
70. Kalekar, L. A. et al. CD4(+) T cell anergy prevents autoimmunity and generates regulatory T cell precursors. *Nat. Immunol.* **17**, 304–314 (2016).
71. Iker Etchegaray, J. et al. Phagocytosis in the retina promotes local insulin production in the eye. *Nat. Metab.* **5**, 207–218 (2023).
72. Ito, Y. et al. Rapid CLIP dissociation from MHC II promotes an unusual antigen presentation pathway in autoimmunity. *J. Exp. Med.* **215**, 2617–2635 (2018).
73. Bettini, M. et al. TCR affinity and tolerance mechanisms converge to shape T cell diabetogenic potential. *J. Immunol.* **193**, 571–579 (2014).
74. Martinez, R. J. & Evavold, B. D. Lower affinity T cells are critical components and active participants of the immune response. *Front. Immunol.* **6**, 468 (2015).
75. Yi, J. et al. Antigen-specific depletion of CD4+ T cells by CAR T cells reveals distinct roles of higher- and lower-affinity TCRs during autoimmunity. *Sci. Immunol.* **7**, eabo0777 (2022).
76. James, E. A., Pietropaolo, M. & Mamula, M. J. Immune recognition of β -cells: neoepitopes as key players in the loss of tolerance. *Diabetes* **67**, 1035–1042 (2018).
77. Lichti, C. F. & Wan, X. Using mass spectrometry to identify neoantigens in autoimmune diseases: The type 1 diabetes example. *Semin. Immunol.* **66**, 101730 (2023).
78. Wenzlau, J. M. et al. Mapping of a hybrid insulin peptide in the inflamed islet β -cells from NOD mice. *Front. Immunol.* **15**, 1348131 (2024).
79. Libman, I. et al. Hydroxychloroquine in stage 1 type 1 diabetes. *Diab. Care* **46**, 2035–2043 (2023).
80. Goginashvili, A. et al. Insulin secretory granules control autophagy in pancreatic β cells. *Science* **347**, 878–882 (2015).
81. Pei, X., Wang, H., Xu, P., Liang, K. & Yuan, L. The core autophagy protein ATG5 controls the polarity of the Golgi apparatus and insulin secretion of pancreatic beta cells. *Biochem. Biophys. Res. Commun.* **629**, 26–33 (2022).
82. Jung, H. S. et al. Loss of autophagy diminishes pancreatic β CELL Mass and Function with Resultant Hyperglycemia. *Cell Metab.* **8**, 318–324 (2008).
83. Zhou, Y. et al. RILP restricts insulin secretion through mediating lysosomal degradation of proinsulin. *Diabetes* **69**, 67–82 (2019).
84. Li, M. et al. VAMP4 regulates insulin levels by targeting secretory granules to lysosomes. *J. Cell Biol.* **221**, e20210164 (2022).
85. Malhotra, D. et al. Tolerance is established in polyclonal CD4(+) T cells by distinct mechanisms, according to self-peptide expression patterns. *Nat. Immunol.* **17**, 187–195 (2016).
86. Legoux, F. P. et al. CD4+ T cell tolerance to tissue-restricted self antigens is mediated by antigen-specific regulatory T cells rather than deletion. *Immunity* **43**, 896–908 (2015).
87. Mingueneau, M., Jiang, W., Feuerer, M., Mathis, D. & Benoist, C. Thymic negative selection is functional in NOD mice. *J. Exp. Med.* **209**, 623–637 (2012).
88. Smith, J. A. et al. Aire mediates tolerance to insulin through thymic trimming of high-affinity T cell clones. *Proc. Natl Acad. Sci. USA* **121**, e2320268121 (2024).
89. Pugliese, A. et al. The insulin gene is transcribed in the human thymus and transcription levels correlated with allelic variation at the INS VNTR-IDDM2 susceptibility locus for type 1 diabetes. *Nat. Genet.* **15**, 293–297 (1997).
90. Vafiadis, P. et al. Insulin expression in human thymus is modulated by INS VNTR alleles at the IDDM2 locus. *Nat. Genet.* **15**, 289–292 (1997).
91. Chentoufi, A. A. & Polychronakos, C. Insulin expression levels in the thymus modulate insulin-specific autoreactive T-cell tolerance. *Diabetes* **51**, 1383–1390 (2002).

92. Culina, S. et al. Islet-reactive CD8+ T cell frequencies in the pancreas, but not in blood, distinguish type 1 diabetic patients from healthy donors. *Sci. Immunol.* **3**, eaao4013 (2018).
93. Atibalentja, D. F., Byersdorfer, C. A. & Unanue, E. R. Thymus-blood protein interactions are highly effective in negative selection and regulatory T cell induction. *J. Immunol.* **183**, 7909–7918 (2009).
94. Vollmann, E. H. et al. Specialized transendothelial dendritic cells mediate thymic T-cell selection against blood-borne macromolecules. *Nat. Commun.* **12**, 6230 (2021).
95. Bonasio, R. et al. Clonal deletion of thymocytes by circulating dendritic cells homing to the thymus. *Nat. Immunol.* **7**, 1092–1100 (2006).
96. Hadeiba, H. et al. Plasmacytoid dendritic cells transport peripheral antigens to the thymus to promote central tolerance. *Immunity* **36**, 438–450 (2012).

Acknowledgements

The authors thank Kodi Ravichandran and Paul Allen for their critical evaluation of the paper and Jennifer Ponce, Christelle Schatz, and Jinsheng Yu for scRNA-seq analysis. We dedicate this study to Marilyn Farquhar, who guided us on the identification of the crinophagic granules, and Bruno Kyewski, who provided crucial advice on assessing thymic antigen presentation by mTECs. This work is supported by the Diabetes Research Center at Washington University (P30 DK020579 to X.W.), the Juvenile Diabetes Research Foundation (5-CDA-2022-1175-A-N to X.W.), and the National Institute of Health (R01AI62591 and R01DK134437 to X.W.).

Author contributions

H.H., L.T., C.F.L., E.R.U., and X.W. designed the study. H.H. and O.J.P. isolated thymus and pancreatic islets. A.N.V. isolated the thymic MHC-II peptidome. H.H., A.N.V., and X.W. performed antigen presentation experiments. H.H. and N.S. performed flow cytometry analysis. H.H. and A.N.V. performed immunization and ELISPOT analysis. A.N.V. isolated β -cell granules. O.J.P. performed diabetes monitoring. W.L.B. performed electron microscopy. T.L. and B.Z. analyzed the single-cell RNA sequencing data. C.F.L. performed the mass spectrometry experiments and analyzed the data. L.K. and L.T. generated I-A^{g7}-based tetramers. C.H. and L.T. critically examined the data and reviewed the paper. X.W. wrote the paper with inputs from all the authors.

Competing interests

The authors declare no competing interests.

Additional information

Supplementary information The online version contains supplementary material available at <https://doi.org/10.1038/s41467-024-52619-5>.

Correspondence and requests for materials should be addressed to Xiaoxiao Wan.

Peer review information *Nature Communications* thanks Remi Creusot and the other anonymous reviewer(s) for their contribution to the peer review of this work. A peer review file is available.

Reprints and permissions information is available at <http://www.nature.com/reprints>

Publisher's note Springer Nature remains neutral with regard to jurisdictional claims in published maps and institutional affiliations.

Open Access This article is licensed under a Creative Commons Attribution-NonCommercial-NoDerivatives 4.0 International License, which permits any non-commercial use, sharing, distribution and reproduction in any medium or format, as long as you give appropriate credit to the original author(s) and the source, provide a link to the Creative Commons licence, and indicate if you modified the licensed material. You do not have permission under this licence to share adapted material derived from this article or parts of it. The images or other third party material in this article are included in the article's Creative Commons licence, unless indicated otherwise in a credit line to the material. If material is not included in the article's Creative Commons licence and your intended use is not permitted by statutory regulation or exceeds the permitted use, you will need to obtain permission directly from the copyright holder. To view a copy of this licence, visit <http://creativecommons.org/licenses/by-nc-nd/4.0/>.

© The Author(s) 2024